International Journal of Greenhouse Gas Control 119 (2022) 103725

Contents lists available at ScienceDirect

International Journal of Greenhouse Gas Control

journal homepage: www.elsevier.com/locate/ijggc

A numerical modelling study to support design of an in-situ CO_2 injection test facility using horizontal injection well in a shallow-depth coal seam

Shakil A. Masum [a,*], Min Chen [a], Lee J. Hosking [b], Kamil Stańczyk [c], Krzysztof Kapusta [c], Hywel R. Thomas [a]

[a] Geoenvironmental Research Centre, School of Engineering, Cardiff University, Cardiff CF24 3AA, UK
[b] Department of Civil and Environmental Engineering, Brunel University London, Kingston Lane, Uxbridge, Middlesex UB8 3PH, UK
[c] Central Mining Institute, Plac Gwarków 1, Katowice 40-166, Poland

ARTICLE INFO

Keywords:
CO_2-storage
Swelling
Injectivity
Modelling
Dual porosity
Horizontal well

ABSTRACT

Previous projects on CO_2 storage in coal often reported the challenges associated with coal swelling and swelling-induced loss of gas injectivity. Since coal seams are typically thin, commonly used vertical wells only intersect a target reservoir over a small contact area, placing constraints on CO_2 injectivity in addition to those resulting from coal swelling. This leaves the storage reservoirs largely under-utilized and, therefore, questions the viability of this technology. To address the challenges/limitations of the current practice, a novel in-situ CO_2 injection test is planned using horizontal injection wells in Mikolow, Poland. This paper presents the pre-operational simulation studies conducted to assist the design and operation of the in-situ test. An existing dual-porosity model that is built on a coupled thermo-hydro-chemical-mechanical (THCM) modelling framework is employed in this study. Sensitivity of the model parameters and validity of the model are tested. Several simulation scenarios are developed in reference to the selected test site for various horizontal well configurations and gas injection conditions. From the results and analyses, it is evident that by varying the coal-CO_2 contact area via the length of the horizontal injection well, as well as the operating conditions including fixed pressure, and fixed rate injection scenarios, the targeted amount (between 1 to 10 tonnes) of CO_2 can be injected into the seam without significant loss of permeability or injectivity, yielding sustained gas injection. Moreover, the spread of CO_2 is predicted to be contained within the model domain suggesting no significant concern of spread exceeding the test area.

1. Introduction

Out of four pathways towards limiting the global temperature rise to 1.5°C, as envisaged by the Paris Agreement on climate change, the Intergovernmental Panel on Climate Change (IPCC, 2018) predicted that three require large scale CO_2 capture and storage (CCS) with cumulative amounts of 348–1218 $GtCO_2$ achieved by 2100. Current rates see only 40 $MtCO_2$ stored per year, indicating that the CCS industry should aim to grow by at least 100-fold in the near future.To control the release of CO_2 in the atmosphere, nations across the world are seeking technology driven greenhouse gas mitigation strategies and, of those, subsurface CCS technologies seem to offer practical solutions (Metz et al., 2005; IEAGHG, 2013).

Large scale CO_2 storage can be achieved in the geological formations, e.g., aquifers, depleted oil and gas reserves, and coal deposits. Coal fileds provide significant CO_2 storage opportunities, and the clusters of large point source CO_2 emitters, especially in Europe, are often collocated with the coal deposits (Vangkilde-Pedersen et al., 2009). The estimated CO_2 storage potential in the coalfields across the globe is around 488 $GtCO_2$ of which 115 Gt is in North America (23.5%), 8.87 Gt is in South and Central America (1.82%), 78.84 Gt is in Europe and Eurasia (16.3%), 29.2 Gt is in Middle East and Africa (5.98%), and 254.91 Gt is in Asia Pacific (52.3%) (IEAGHG, 2013). The candidate coalfields in Europe spread across the United Kingdom, Belgium, the Netherlands, Germany, Poland, and Hungary, Spain and France (Alves Dias et al., 2018). Poland has the highest coalfield CO_2 storage potential with an estimated capacity up to 1254 Mt, accompanied by the Czech Republic (118-380 Mt), Hungary (68-427 Mt), the Netherlands (300 Mt), Spain (145 Mt), the South Wales Coalfield, UK (105 Mt), Italy (71 Mt), and Bulgaria (17 Mt) (Vangkilde-Pedersen et al., 2009; Alves Dias et al., 2018; EU Geocapacity, 2008; Sarhosis et al., 2016). To exploit the potential and the usage of coal seams as CO_2 storage reservoirs, a number

* Corresponding author.
E-mail address: masumsa1@cf.ac.uk (S.A. Masum).

https://doi.org/10.1016/j.ijggc.2022.103725
Received 3 December 2021; Received in revised form 15 June 2022; Accepted 29 June 2022
Available online 6 July 2022

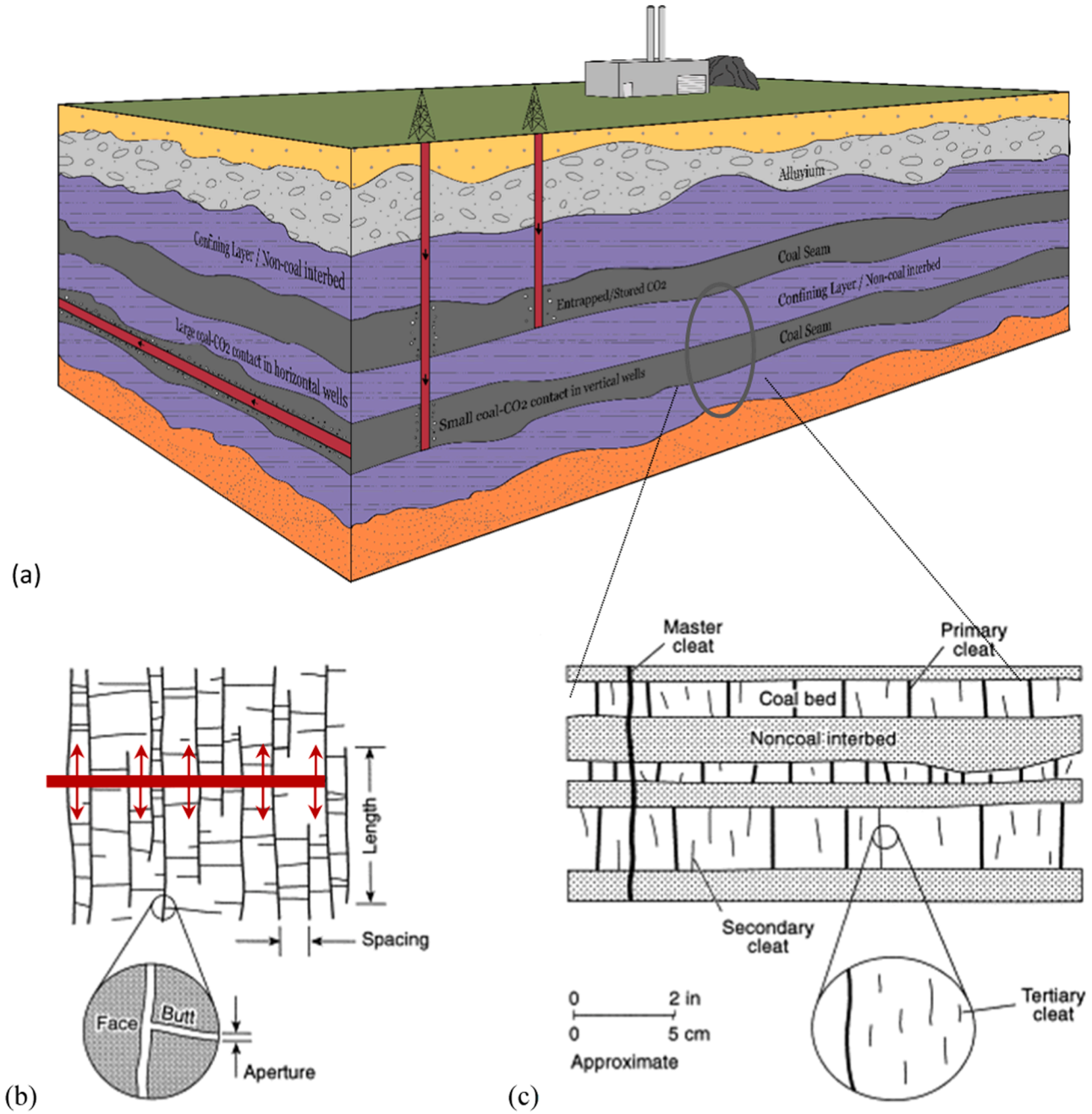

Fig. 1. (a) Illustration of CO_2 storage in subsurface coal deposits. Generalised coal cleat geometry, (a) Plan view, and (b) Cross-section view (Laubach et al., 1998). The optimal layout for a horizontal well with the associated hydraulic connection to the face cleats is indicated in (b).

of pilot projects have been conducted across the globe. Pilot project and demonstration experience of CO_2 storage and utilisation has been gained steadily since the earliest project conducted between 1995 and 2001 in the San Juan Basin (Allison Unit) in the USA. This was conducted as part of the US Department of Energy Regional Carbon Sequestration Partnership programme and was the largest by far, involving the injection of 251,000 t of CO_2 at a depth of 950 m. Subsequent projects have involved smaller amounts of CO_2 as summarised in the Appendix Table A1.

The previous projects often reported technical challenges associated with CO_2 injection in coal, particularly, problems in achieving a sustained, practical rate of injection (RECOPOL, 2006; Fujioka et al., 2010), owing to the permeability loss caused by CO_2 sorption-induced coal swelling. The physicochemical interaction between the coal matrix and CO_2 gas molecules causes the matrix to swell. Coal is a naturally fractured medium with distinct matrix blocks separated by well defined fracture networks, also known as cleats (Harpalani and Chen, 1997). While the cleats provide the major conduits for gases and liquids flow, the coal matrix with its large pore surfaces provide the sites for gas adsorption. Under subsurface conditions, swelling of the coal matrix constricts the flow channels, i.e., reduces the fracture permeability, which eventually results in a loss of gas injectvity, as experienced in the past projects. Coal swelling is nearly proportional to the amount of adsorbed CO_2 in its matrix (White et al., 2005). CO_2 storage potential is evident in all coal ranks, however, the capacity varies with rank and operation conditions, e.g., pressure, temperature, confinement, moisture content, etc. CO_2 sorption capacity of dry coals reduces with increasing rank, reaches to a minimum, and then increases again with rank (Busch and Gensterblum, 2011). This is due to the fact that micropores provide most of the surface area for gas adsorption, and microporosity becomes predominant in high-rank coals. Gas adsorption

capacity of coal generally increases with pressure, but decreases with increasing temperature (Cai et al., 2014) and confining pressures (Pone et al., 2009). Coals with high cleat density exhibit greater degree of swelling, and the density is generally higher in high-rank coals (Perera et al., 2011). Although the density increases from lignite or sub-bituminous to bituminous coal, it decreases afterwards up to anthracite (Perera, 2017). Coal swelling also follows this trend with the coal rank (Perera, 2017; Walker et al., 1988). From the theoretical point of view, high rank coal deposits at deeper subsurfaces seem to provide better and safer storage of injected CO_2. However, higher swelling and confinment pressures, first and foremost, make it less practical from a CO_2 injection point of view. In such cases, a principal concern is the need for over-pressurisation or high pressure fractruing of the seams for successful gas injection operations (RECOPOL, 2006), leading to concerns over caprock integrity and leakage.

Coal cleats are categorised as more continuous face cleats and less continuous butt cleats (Fig. 1), which are mutually perpendicular and in turn perpendicular to the bedding plane (Ammosov and Eremin, 1963; Tremain et al., 1991; Laubach et al., 1998). Face cleats extend along the direction of horizontal maximum principal stress (Su et al., 2001) and provide the primary flow pathways. Aligning gas injection wells in a way such that they intersect many face cleats is therefore likely to establish the best possible connection with these dominant flow pathways (Fig. 1b). However, the majority of the past projects used vertical injection wells to supply gas to the seams. Since coal seams are typically thin, the vertical wells only intersect the target reservoir over a small contact area (Fig. 1a), placing constraints on CO_2 injectivity in addition to those resulting from coal swelling. This leaves the storage reservoirs largely under-utilized and, therefore, questions the viability of CO_2 storage in coal seams, especially using vertical injection wells. Horizontal wells have been considered for investigating coal bed methane recovery in many numerical simulation studies (Gentzis and Bolen, 2008; Ren et al., 2014; Sheng, 2017; Zhang et al., 2020; Connell et al., 2014). However, their field applications are rarely reported (Zhang et al., 2020), especially, for sole CO_2 injection and storage projects/studies that ignore the coal bed methane recovery, and there is a notable gap in the literature. There is an imperative need to advance the technological aspects of a novel CCS strategy in coal, overcoming the reported issues.

This manuscript presents the pre-operational simulation studies conducted to assist the design and operation of the in-situ test facility. Between 1 to 10 t of CO_2 is planned to be injected at the experimental test site, Mikolow, Poland, which has been selected under the ongoing ROCCS project (www.roccsproject.com). A comparison of the key features of the ROCCS project with the other demonstration projects in Europe is listed in Appendix Table A2. The target coal-seam is at a shallow depth, 30 m, from the surface and already de-methanised. Evidence of pilot CO_2 injection tests at such shallow level coal seams, using horizontal injection wells, is rare. In this work, potential of the shallow coal-seam for safe CO_2 storage is investigated. The aim is to establish a set of design recommendations that are site-specific and ensures safe and sustained gas injection, during the in-situ test, circumventing the need for over-pressurisation or hydraulic fracturing and minimising gas leakage. An appropriate combination of the coal-CO_2 contact length, i.e., the horizontal injection well length, and CO_2 injection conditions is essential to achieve the proposed CO_2 injection. Several site-specific simulation scenarios are developed, for which the swelling-induced loss of coal permeability, amount of adsorbed CO_2, and propagation of the gas in the study area are assessed. Two injection-well concepts are tested to support the design of the horizontal well. The theoretical background of the numerical model is presented in detail. Validity of the model is tested against a laboratory experiment on CO_2 sorption induced coal swelling and permeability evolution. Sensitivity of the model parameters is examined for identifying the key site and coal-gas interaction information. Simulation results are analysed and discussed comprehensively to establish a set of design recommendations for the in-situ test.

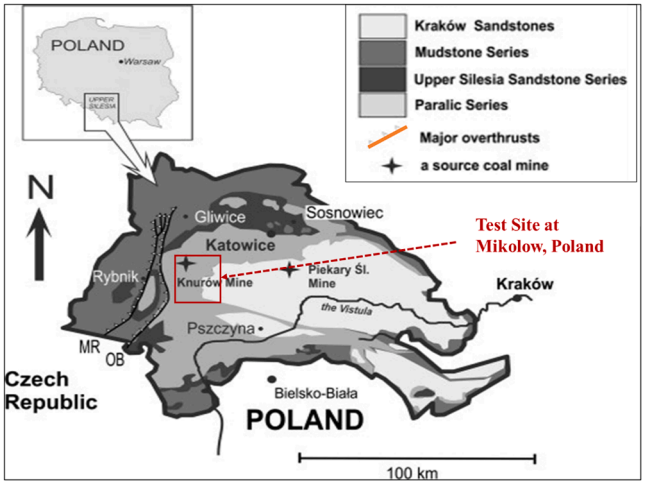

Fig. 2. Geological map of Upper Silesian Coal Basin and the location of the Experimental Mine Barbara (EMB) in Mikołów, Poland (*after* Fabiańska & Smółka-Danielowska, 2012).

2. The *in-situ* test site

The ROCCS in-situ test site at the Experimental Mine Barbara, (EMB), Mikołów, is located within the Upper Silesian Basin, Poland (Fig. 2). In the geology of the mining area, Quaternary formations, represented by Orzesze Beds, overlap discontinuous Carboniferous layers, represented by Laziska Beds (Kapusta et al., 2013). Most of the mining area resides directly under the Orzesze Beds containing silty shale, fine and medium grained sandstone, and hard coal seams. The Laziska Beds contain sandstones and conglomerates. The average depth of the target coal seam is 30 m, with thickness of 1.5 to 2.0 m, and an angle of dip between 4 and 6° (Kapusta et al., 2013). The depth is shallower (30 m) than those targeted by the other pilot projects, *e.g.*, MOVECBM (van Wageningen et al., 2009) and CARBOLAB (Lafortune et al., 2014), but it is nonetheless suitable for the main purpose of investigating the relationship between CO_2 injectivity and coal-CO_2 contact area. This is set in the context of broadly exploring whether shallower seams can offer an improved balance of storage capacity, injectivity, storage security, and cost. Whilst it is expected that storage capacity is lower, adsorption still provides storage security, there is no need for over-pressurisation or permeability stimulation for a sustained injection rate, and the facility cost will be significantly lower. In other words, there is potential for facilities that are smaller in scale but much more repeatable, especially since the decline of coal mining increasingly leaves shallow seams available for new low carbon developments.

Within the EMB, the "seam-310" is selected as the target coal seam for the ROCCS *in-situ* CO_2 injection test. The location of "seam-310" with its map of underground mine workings is shown in Fig. 3. The exact location of the test site is highlighted inset. The coal is sub-bituminous. No major faults or large geological fissures exists in the test area. The heterogeneity of geological properties arises from micro and macro-fissures and interchangeable layers of mudstone and sandstone. The deposits at EMB have been already de-methanised, and methane doesn't appear in the galleries anymore. The overburden strata at the EMB (which consists of both carbonaceous and non-carbonaceous silt layers) is highly impermeable and provide sufficient insulation to upward gas flow.

3. Materials and methods

The numerical simulations are performed using a bespoke model, namely, COMPASS (**CO**de for **M**odelling **PA**rtially **S**aturated **S**oils)

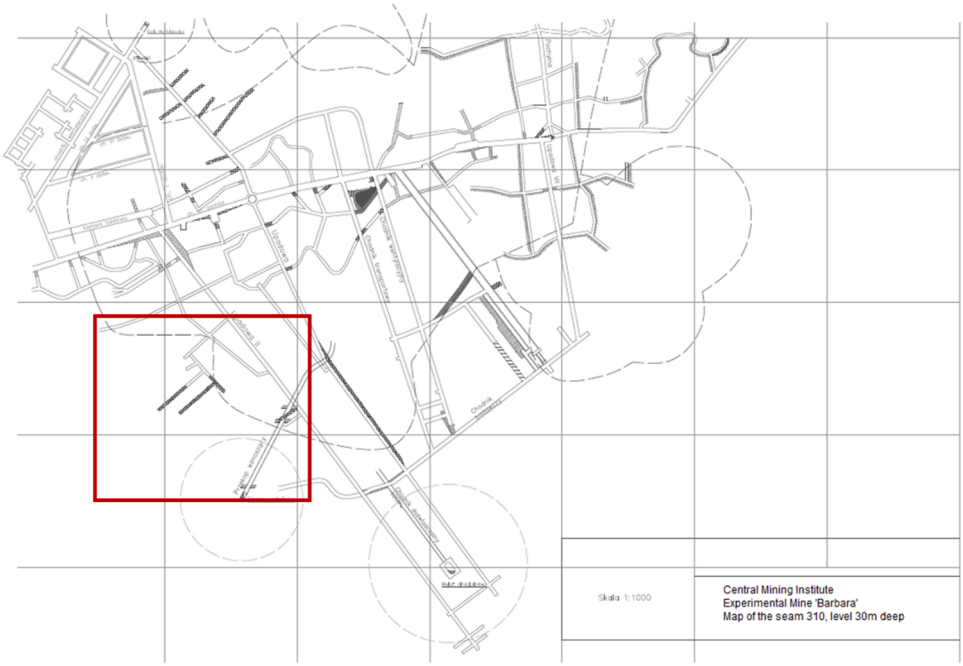

Fig. 3. The map of seam-310 with underground workings in the Experimental Mine Barbara and the location of the test area (inset). A higher resolution map of the seam-310 is available at: https://www.roccsproject.com/test-site.

(Thomas and He, 1995; Thomas et al., 2011; Masum, 2012; Hosking, 2014; Masum and Thomas, 2018, 2021; Hosking et al., 2020) that is built on a coupled thermo-hydro-chemical-mechanical (THCM) modelling framework. It analyses thermal, hydraulic, gas, chemical, biological, and mechanical displacement behaviours of subsurface porous materials. The governing equations of flow, reaction, and deformation in the model are developed following a mechanistic approach where various mechanisms of the behaviours are included in an additive manner with appropriate couplings as required. The code facilitates dual porosity modelling and advanced hybrid discrete fracture-dual porosity modelling capabilities as detailed in (Hosking, 2014; Hosking et al., 2020; Chen, 2019; Chen et al., 2022, 2019, 2020a, 2020b, 2020c). The fracture network and the matrix blocks in coal are treated as distinct continua with a coupled mass transfer interface between the two continua. In the subsequent sections, the fracture continuum and the matrix continuum are denoted by subscripts *f*, and *m*, respectively. The model formulations represent multiphase flows through elastically deformable fractured rocks relevant to CO_2 sequestration in coal. The following assumptions are made: (i) gas exists as free phase in the fractures, whereas it exists as both free phase and adsorbed phase in the matrix; (ii) adsorption behaviour follows Langmuir isotherm; (iii) coal is isotropic and elastic; (iv) the system is isothermal, and (v) the effect of gravity is negligible.

3.1. Governing equations

3.1.1. Theory of gas transport in coal

Gas transport in coal fracture/matrix continuum (Ω) is expressed as:

$$\frac{\partial}{\partial t}\left(c_{g\Omega}\theta_{g\Omega}\right)+\frac{\partial}{\partial t}\left(c_{d\Omega}\theta_{w\Omega}\right)=-\nabla\cdot\left(c_{g\Omega}\mathbf{v}_{g\Omega}-\mathbf{D}_{g\Omega}\cdot\nabla c_{g\Omega}\right)+R_{g\Omega}+\Gamma_{g\Omega} \tag{1}$$

where $c_{g\Omega}$ is the concentration of free gas and $c_{d\Omega}$ is the concentration of dissolved gas in pore liquid, in the $\Omega = f$ and the $\Omega = m$, i.e., the fracture and matrix continuum. $\theta_{g\Omega}$ is the volumetric gas content, $\theta_{w\Omega}$ is the volumetric water content, $\mathbf{v}_{g\Omega}$ is the gas velocity, $\mathbf{D}_{g\Omega}$ is the effective gas diffusivity, in Ω-continuum. $R_{g\Omega}$ is the sink-source term, and $\Gamma_{g\Omega}$ is the gas exchange rate between the matrix and fracture continua. In dry coal $\theta_{g\Omega} = n_\Omega$ where n_Ω is the porosity of continuum Ω_f or Ω_m. In unsaturated/partially saturated coal, where both gas and liquid phases exists simultaneously, the volumetric contents are related to their individual phase saturation levels, i.e., degree of liquid saturation ($S_{w\Omega}$) or degree of gas saturation ($S_{g\Omega}$)as:

$$\theta_{g\Omega} = n_\Omega S_{g\Omega} \tag{2a}$$

$$\theta_{w\Omega} = n_\Omega S_{w\Omega} \tag{2b}$$

$$S_{g\Omega} + S_{w\Omega} = 1 \tag{2c}$$

It is well established that fluid flow in coal fractures is pressure driven (or advective); while in the matrix it is concentration driven (or diffusive). This is because matrix permeability is significantly smaller than the fracture permeability and, therefore, advection in Ω_m is generally neglected, i.e., $\mathbf{v}_{gm} \approx 0$. Darcy's law is applied to Ω_f as:

$$\mathbf{v}_{gf} = -\frac{K_f K_{rgf}}{\mu_g}\nabla p_{gf}. \tag{3}$$

Here K_f is the intrinsic permeability, K_{rgf} is the gas-phase relative permeability in Ω_f, μ_g is gas viscosity, and p_{gf} is the pressure of free gas-phase in fractures. In dry coal, $K_{rgf} = 1$ and in partially saturated coal it depends on the degree of liquid or gas saturation.

The mass exchange rate ($\Gamma_{g\Omega}$) between the fracture and matrix continua is expressed as:

$$\Gamma_{gf} = -\Gamma_{gm} = -\frac{1}{\tau}\left(c_{gf} - c_{gm}\right) \tag{4}$$

where τ is diffusion time.

The sink/source term $R_{g\Omega}$, calculates the amount of bulk gas lost into or gained from the adsorbed phase. Gas adsorption in coal fractures is negligible in comparison to its matrix, *i.e.*, $R_{gf} \approx 0$. Gas sorption in coal follows a Langmuir isotherm. Therefore:

$$R_{gm} = -\frac{d(\rho_s c_s)}{dt} \tag{5}$$

$$c_s = \frac{C_L p_{gm}}{p_{gm} + p_L} \tag{6}$$

where c_s is the concentration of adsorbed gas in the coal matrix, ρ_s is coal density, C_L is the Langmuir volume constant, $p_L$is the Langmuir pressure constant. p_{gm} represents the free gas pressure in Ω_m and, for non-ideal or real gases:

$$p_{gm} = Z_m R T c_{gm}. \tag{7}$$

Here, R is the universal gas constant, T is absolute temperature, and Z_m is the gas compressibility factor in the matrix continuum, which is calculated with the equation of state proposed by Peng and Robinson (Peng and Robinson, 1976).

Assuming a thermodynamic equilibrium between the dissolved gas and the free gas, the concentration of the dissolved gas can be obtained as:

$$c_{d\Omega} = H_g c_{g\Omega} \tag{8}$$

where H_g is the Henry's coefficient.

Substitution of Eqs. (2)-(8) into Eq. (1) and re-arrangement yields the governing equations of gas transport in coal.

The governing equations of gas transport in fracture continuum (Ω_f):

$$C_{c_{gf}c_{gf}} \frac{\partial c_{gf}}{\partial t} = \nabla\left(K_{c_{gf}c_{gf}} \nabla c_{gf}\right) + Q_{c_f} \tag{9}$$

$$C_{c_f c_f} = n_f S_{gf} + n_f H_g S_{wf} \tag{9a}$$

$$K_{c_f c_f} = c_f R Z_f T \frac{K_f K_{rgf}}{\mu_{gf}} + D_{gf} \tag{9b}$$

$$Q_{c_f} = -\frac{1}{\tau}\left(c_f - c_m\right) \tag{9c}$$

The governing equations of gas transport in matrix continuum (Ω_m):

$$C_{c_{gm}c_{gm}} \frac{\partial c_{gm}}{\partial t} = \nabla\left(K_{c_{gm}c_{gm}} \nabla c_{gm}\right) + Q_{c_m} \tag{10}$$

$$C_{c_{gm}c_{gm}} = n_m S_{gm} + n_m H_g S_{wm} + \rho_s \frac{\partial c_s}{\partial c_{gm}} \tag{10a}$$

$$K_{c_{gm}c_{gm}} = D_{\mathrm{gm}} \tag{10b}$$

$$Q_{c_m} = \frac{1}{\tau}\left(c_f - c_m\right) \tag{10c}$$

3.1.2. Theory of coal deformation

For quasi-static conditions, the linear momentum balance equation for a representative elementary volume of a fractured porous medium can be reduced to equilibrium total stress equations (Jaeger et al., 2009):

$$\mathbf{B}^T d\sigma + F = 0 \tag{11}$$

$$\mathbf{B}^T = \begin{bmatrix} \frac{\partial}{\partial x} & 0 & 0 & \frac{\partial}{\partial y} & 0 & \frac{\partial}{\partial z} \\ 0 & \frac{\partial}{\partial y} & 0 & \frac{\partial}{\partial x} & \frac{\partial}{\partial z} & 0 \\ 0 & 0 & \frac{\partial}{\partial z} & 0 & \frac{\partial}{\partial y} & \frac{\partial}{\partial x} \end{bmatrix} \tag{11a}$$

where σ is the component of total stress tensor and F is the body force vector.

According to Biot's effective stress law, the total stress can be expressed in terms of the effective stress and the average pore pressure as:

$$d\sigma' = d\sigma - \alpha_m \mathbf{I} dp_m - \alpha_f \mathbf{I} dp_f \,. \tag{12}$$

Here, σ' is the effective stress tensor, α_f and α_m are the phenomenological constants, termed as modified Biot's coefficients. p_m and p_f are the average pore pressures of matrix and fracture continuum, respectively. For unsaturated fractured rocks, the average pore pressure is weighted by the liquid and gas saturations (Lewis and Schrefler, 1998; Pao and Lewis, 2002) as:

$$p_m = S_{wm} p_{wm} + S_{gm} p_{gm} \tag{13a}$$

$$p_f = S_{wf} p_{wf} + S_{gf} p_{gf} \tag{13b}$$

where p_{wm} and p_{wf} are the pore liquid pressures in the matrix and in the fracture, respectively. They are considered zero in dry coal. The phenomenological constants α_f and $\alpha_m$can be obtained in terms of physically measurable mechanical parameters (Pao and Lewis, 2002, Lewis and Pao, 2002):

$$\alpha_f = 1 - \frac{K}{K_m} \tag{14a}$$

$$\alpha_m = \frac{K}{K_m} - \frac{K}{K_s}. \tag{14b}$$

Here, $K = E/3(1-2\nu)$ is the bulk modulus of a fractured rock, $K_m = E_m/3(1-2\nu)$, is the bulk modulus of coal matrix, and K_s is the modulus of the coal solids. E is the bulk Young's modulus; E_m is the Young's modulus of the coal matrix, which is obtained experimentally from the specimens that are an order of magnitude larger than the spacing of the matrix pores but devoid of fracture. ν is the Poisson's ratio.

The stress-strain constitutive relation is defined as:

$$d\sigma' = D d\varepsilon^e \tag{15}$$

where D is the elastic stiffness tensor, and $\varepsilon^e$is the elastic strain vector. The total strain, ε, is expressed as:

$$d\varepsilon = d\varepsilon^e + \frac{1}{3}\mathbf{I} d\varepsilon^s + \frac{1}{3}\mathbf{I} d\varepsilon^T \tag{16}$$

where ε^s is the sorption-induced volumetric strain, and ε^T is thermal expansion-contraction strain. The strain-displacement relation is written as:

$$d\varepsilon = \mathbf{B} d\mathbf{u} \tag{17}$$

where $\mathbf{B}$ is the strain-displacement matrix and $\mathbf{u}$ is the solid displacement vector.

The total adsorption-induced strain is calculated as:

$$\varepsilon^s = -\frac{\alpha_m u_a}{K} \tag{18a}$$

$$u_a = -\varphi \Gamma^{max} R T \ln\left(1 + \frac{p_{gm}}{p_L}\right). \tag{18b}$$

Here, Γ^{max} is the Langmuir adsorption constant, representing the adsorption capacity of fluid per unit adsorption surface, and φ is a constant material parameter representing the correlations between changes in the adsorption area of the matrix pore and in porosity of the matrix. In this study, Γ^{max} and φ are lumped together and obtained by matching experimental data.

The thermal strain caused by temperature increases or decreases can be defined as:

$$\varepsilon^T = \alpha_T (T - T_0) \tag{19}$$

where α_T is thermal expansion coefficient. Therefore, $d\varepsilon^s$ and $d\varepsilon^T$ in Eq. (16) can be expressed as:

$$d\varepsilon^s = \frac{\partial \varepsilon^s}{\partial c_m} dc_m + \frac{\partial \varepsilon^s}{\partial T} dT = A^s_{c_m} dc_m + A^s_T dT \tag{20a}$$

$$d\varepsilon^T = \alpha_T dT \tag{20b}$$

where $A^s_{c_m} = \frac{\alpha_m \Gamma^{max} Z_m R^2 T^2}{K(p_L + p_{gm})}$ and due to isothermal condition, $\varepsilon^T = 0$.

Substitution of Eqs. (12)-(20) into Eq. (11) and the re-arrangement yields the governing equations of coal deformation including adsorption-induced swelling strains.

The governing equations of coal deformation:

$$C_{\mathbf{u}c_{gf}} dc_{gf} + C_{\mathbf{u}c_{gm}} dc_{gm} + C_{\mathbf{uu}} d\mathbf{u} = 0 \tag{21}$$

$$C_{\mathbf{u}c_{gf}} = \mathbf{B}^T \mathbf{I} \alpha_f S_{gf} Z_f RT \tag{21a}$$

$$C_{\mathbf{u}c_{gm}} = \mathbf{B}^T \mathbf{I} \alpha_m S_{gm} Z_m RT - \frac{1}{3} \mathbf{B}^T D \mathbf{I} A^s_{c_m} \tag{21b}$$

$$C_{\mathbf{uu}} = \mathbf{B}^T D \mathbf{B} d\mathbf{u} \tag{21c}$$

3.1.3. Constitutive relationships of swelling-induced porosity and permeability evolution

Fracture permeability is generally controlled by the characteristics of fracture network including fracture opening, intensity, tortuosity, and connectivity. Considering these factors, the fracture permeability is given as (Chen et al., 2015):

$$K_f = \frac{R_c}{\tau_f} D \frac{b^3}{12} \tag{22}$$

where τ_f is a tortuosity parameter, R_c fracture connectivity coefficient, D is the fracture intensity and b is the fracture aperture.

The fracture porosity, n_f, can be estimated as:

$$n_f = bA \tag{23}$$

where A is area of fractures per unit volume of rock. Substituting Eq. (23) into Eq. (22) yields:

$$K_f = \frac{R_c}{\tau_f} \frac{D}{A^3} \frac{{n_f}^3}{12} \tag{24}$$

Differentiating Eq. (24) with respect to mean stress and re-arrangement yields:

$$dK_f = \frac{R_c}{\tau_f} \frac{D}{A^3} \frac{{n_f}^3}{4} \frac{\partial n_f}{n_f \partial \bar{\sigma}} d\bar{\sigma}. \tag{25}$$

Here, $\bar{\sigma}$ is the mean effective stress in fractures.

The directional fracture compressibility is defined as:

$$C_f = -\frac{\partial n_f}{n_f \partial \bar{\sigma}} \tag{26}$$

Substituting Eqs. (24) and (26) into Eq. (25) results into:

$$\frac{dK_f}{K_f} = -C_f d\bar{\sigma} \tag{27}$$

Therefore, the fracture permeability can be obtained by integrating Eq. (27) which yields:

$$K_f = K_{f0} e^{-3\left[C_f \Delta \bar{\sigma}\right]} \tag{28}$$

where k_{f0} is the fracture permeability at the reference stress state.

The fracture compressibility is stress- and gas adsorption-dependent (Sampath et al., 2019). Therefore:

$$C_f = C_{f0} \left(\frac{1 - e^{-\alpha_c \bar{\sigma}}}{\alpha_c \bar{\sigma}} \right) \left[\frac{1}{\left(1 - \frac{\gamma p_{gm}}{p_{gm} + p_L} \right)} \right]. \tag{29}$$

Here, C_{f0} is the initial fracture compressibility, α_c is the fracture compressibility change rate, and γ is a weakening coefficient that estimates the effect of coal-gas interaction on the coal compressibility. Eq. (29) describes the influence of both effective stress and gas adsorption on fracture compressibility. According to cubic law, the porosity can be obtained:

$$\left(\frac{n_f}{n_{f0}} \right) = \left(\frac{K_f}{K_{f0}} \right)^{1/3} \tag{30}$$

The numerical solutions of the governing equations presented in Section 3.1 are achieved by applying the Galerkin finite element method for spatial discretisation and by an implicit mid-interval backward-difference scheme for temporal discretisation.

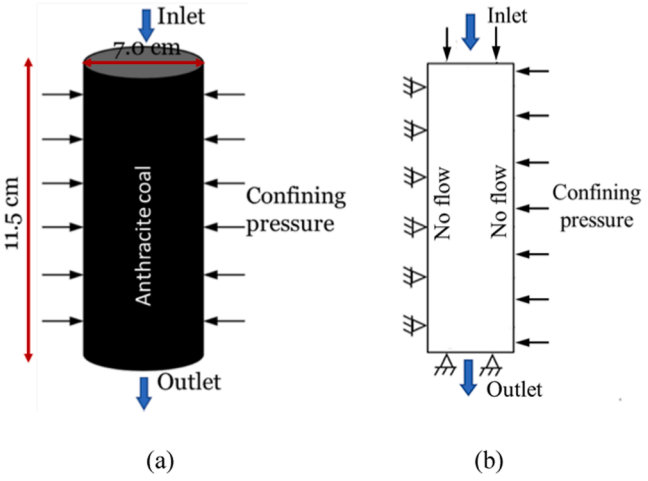

Fig. 4. (a) Laboratory specimen and the experimental boundary conditions, (b) the model domain and the assigned boundaries for validating the model against the coal permeability data of Zagorscak (2017).

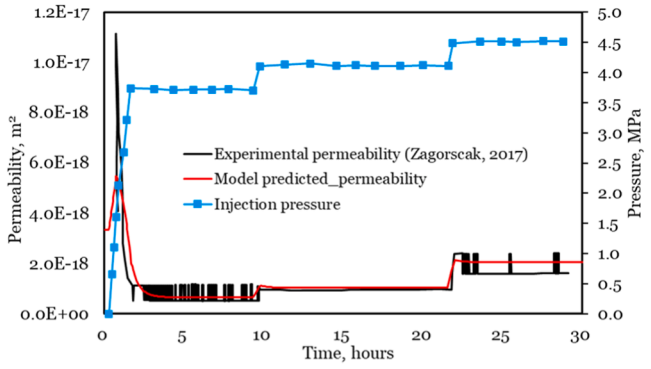

Fig. 5. Comparison between the model predicted permeability result with that of the experimental data of Zagorscak (2017).

3.2. Model validation

Extensive verification and validation of the applied dual porosity model has been presented elsewhere (Hosking et al., 2020; Chen, 2019; Chen et al., 2022, 2019, 2020a, 2020b, 2020c). Within the scope of this work, an additional validation of the model is performed to demonstrate the reliability and accuracy of the presented model. Laboratory experiments on subcritical CO_2 injection, sorption, and swelling-induced permeability loss in dry anthracite coal samples were conducted by Zagorscak (2017). Cylindrical specimens of 7.0 cm diameter and 11.5 cm length were prepared from the samples collected from a coalfield in the South Wales, UK. CO_2 was injected at 3.8 MPa, 4.2 MPa, and 4.6 MPa under a confining pressure of 5.1 MPa and temperature 311 K. Flow rates were recorded throughout the experiments to measure the permeability variations of the specimens. Zagorscak (2017) collected the

Table 3
The model parameters used in the validation exercise.

Parameters	Value	Reference
Young's modulus of coal, E (GPa)	1.6	(Zagorscak, 2017)
Poisson's ratio, ν (-)	0.4	,,
Initial permeability, k_{f0} (m^2)	1.6×10^{-17}	,,
Initial matrix porosity n_m (-)	0.025	,,
Initial fracture porosity n_f (-)	0.01	,,
Density of coal, ρ_c (kg/m^3)	1376	,,
Viscosity of gas, μ_g (Pa•s)	1.1×10^{-5}	,,
Langmuir volume constant, V_L (mol/kg)	1.9	,,
Langmuir pressure, P_L (MPa^{-1})	0.91	,,
Sorption time, τ (h)	0.42	,,
Formation temperature, T (K)	311	,,
Fracture compressibility at reference state, C_{f0} (MPa^{-1})	0.2	Fitted
Fracture compressibility change rate, α_c, (MPa^{-1})	0.15	Fitted
Weakening coefficient, γ (-)	0.9	Fitted

permeability evolution data, at the inlet boundary of the specimens, which is used here to validate the current model.

The model domain and the boundary conditions of this validation exercise are shown in Fig. 4. The experimental conditions are as follows: the initial gas pressure in the specimen is 0.1 MPa. A zero-flux boundary is applied to the right and left boundaries of the domain. The time-dependent injection pressure curve (Fig. 5) is used at the inlet boundary and a constant backpressure of 0.1 MPa is applied at the outlet boundary. For deformation, the vertical displacement at the outlet boundary is constrained and a constant confining stress is assigned to the inlet and to the lateral boundary, as shown in Fig. 4(b).

The parameters used in this test are listed in Table 3. Properties of the coal samples and the gas adsorption parameters are collected from Zagorscak (2017). The initial fracture compressibility (C_{f0}), fracture compressibility change rate (α_c), and the weakening coefficient (γ) associated with coal-CO_2 interactions are obtained by matching the experimental data. The calculated fracture compressibility of 0.2 MPa^{-1} is in the range, 0.06 - 0.687 MPa^{-1}, reported in the literatures (Chen et al., 2011; Zheng et al., 2012; Peng et al., 2017). The fitted value of α_c is 0.15 MPa^{-1}, which is in the range (0.1 - 0.9 MPa^{-1}) estimated by Connell (2016). The value of γ is 0.9, which means that the sorption of CO_2 greatly softens the anthracite coals. This is consistent with the significant reduction of the compressive strengths reported by Zagorscak (2017).

The experimental data and its comparison with the model result are shown in Fig. 5. The model predicted result is in good agreement with the experimental result. This suggests that the CO_2 sorption in coal and the associated swelling-induced loss of permeability can be evaluated with good confidence by the model. During the experiment, permeability of the coal reduced significantly, from 1.6×10^{-17} m^2 to 1.0×10^{-18} m^2, estimating a 93.7% loss from the initial permeability. To keep the injection running, the gas pressure was increased from the initial 3.8 MPa to 4.2 MPa and then to 4.6 MPa. CO_2 sorption in coal and the swelling-induced permeability and injectivity loss experienced in the laboratory experiment, were also experienced by the previous pilot projects on CO_2 storage in coal deposits.

4. Model development

4.1. Injection well design concept

The design of the CO_2 injection well requires that the coal-CO_2 contact area can be controlled to determine its relationship with the gas injectivity, thereby, to evaluate the improved connectivity with preferential flow pathways formed by the local heterogeneities within the natural fracture network. Two design concepts are tested here. Considered first is the use of open-hole packers at fixed intervals using a Packer-and-Port concept (Fig. 6a) that allows zonal isolation to control flow through the seam. The concept is based on the assumptions that the ports can be controlled individually, and the distance between the individual packers/ports is known prior to the gas injection. Considered second as an alternative or equivalent concept is to drill horizontal injection wells of variable lengths or increasing lengths in stages (Fig. 6b). Both design options are studied and assessed to aid the design of the in-situ gas injection system.

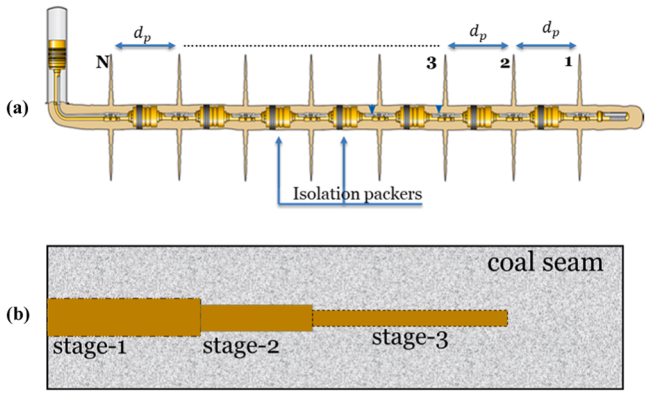

Fig. 6. Schematics of (a) Packer-and-Port open-hole zonal isolation (Energy, and Environmental Research Center, 2014) concept, and (b) alternative (staged drilling) concept for incremetnal control of coal-CO_2 contact area.

4.2. The model domains

The area of the coal seam where the in-situ test will be conducted is marked as the "test area" in the inset of Fig. 3. Considering the existing infrastructure and the current underground mine workings, the selected width of the study area is 35 m. The length of the study domain is variable, and it depends on the length of the injection well. The first part

Table 4
Summary of the simulation scenarios and scenario ID.

Injection well system		Gas injection conditions		
		Fixed pressure	High injection rate	Low injection rate
Design 1	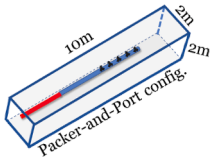	-	**D1B2**	**D1B3**
Design 2	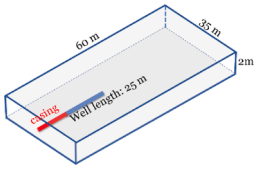	**D2B1**	**D2B2**	**D2B3**
Design 3	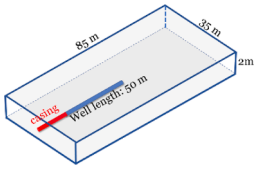	**D3B1**	**D3B2**	**D3B3**
Design 4	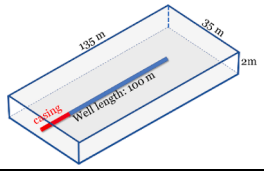	**D4B1**	**D4B2**	**D4B3**

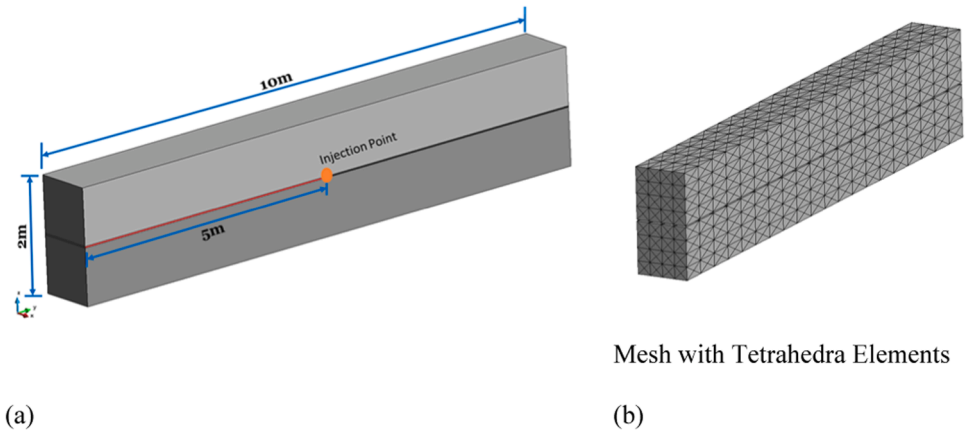

Fig. 7. (a) The model domain and (b) finite element meshing for Design 1 simulation.

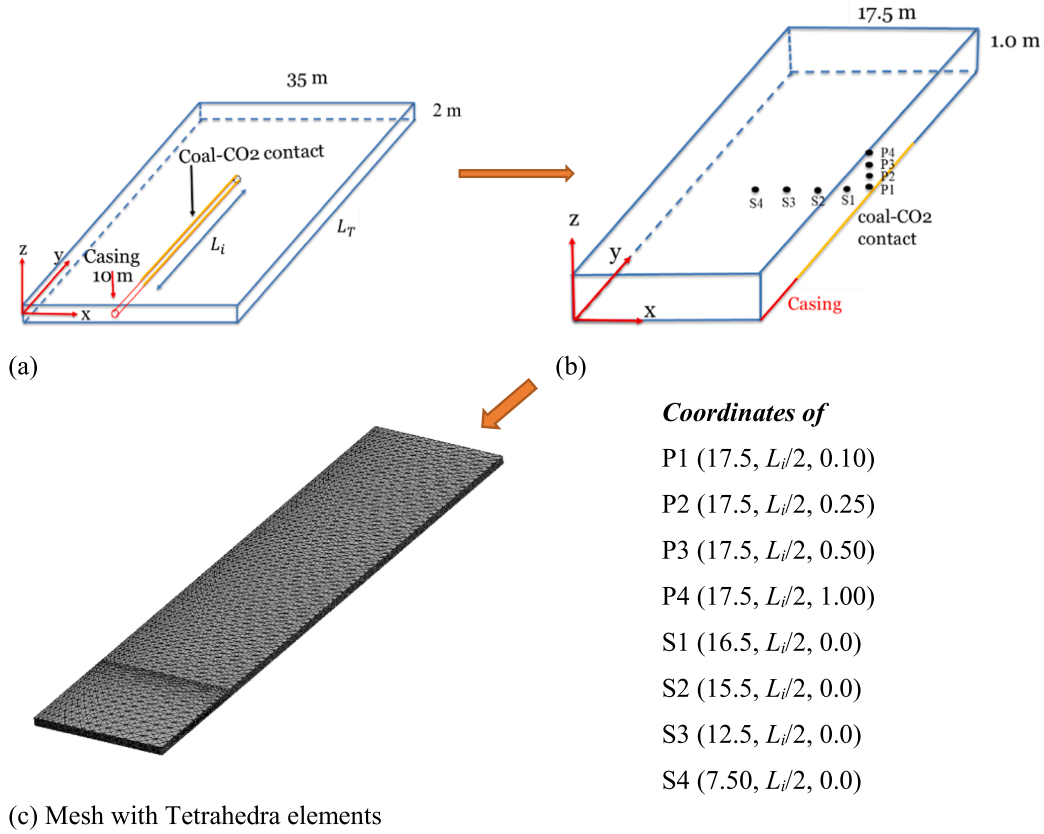

Fig. 8. (a) The model domain, (b) simulation domain, and (c) discretised domain for Design 2 - 4 simulations. The total legnth (L_T) includes 10 m cased well, variable coal-CO_2 contact, and 25 m intact seam. The coal-CO_2 contact length (L_i) of Design 2, 3, and 4 are 25 m, 50 m, and 100 m, respectively. P1 to P4 are the locations of the observation points along the vertical z-axis, and S1 to S4 are along the horizontal x-axis.

of the injection well will be lined with casing to stop gas leakage at the vicinity of the gallery. The length of the study domain, therefore, combines the length of the cased well, the length of the well that is in contact with coal seam (coal-CO_2 contact length), plus 25 m of the intact seam. The depth of the model domain is 2 m, which represents the thickness of seam-310.

Four design options are considered in this study. Design 1 represents the Packer-and-Port concept, and the Designs 2 to 4 represent the alternative concept of variable injection lengths. The in-seam coal-CO_2 contact length in Designs 2, 3, and 4 are 25 m, 50 m, and 100 m, respectively.

4.3. Gas injection conditions

The project plans to inject between 1,000 to 10,000 kg of CO_2 during the in-situ test. Herein, three gas injection boundary conditions, namely, a fixed pressure boundary (B1) and two constant injection rate boundaries (B2 and B3) are investigated. The duration of the in-situ test is 6 months and at the high injection rate (B2) of 2.0 kg/h, a total of 8640 kg of CO_2 can be injected into the seam. At the low injection rate (B3) of 0.5 kg/h, this equates to 2160 kg of CO_2. The fixed boundary pressure (B1) of 5 bar injects approximately 20,000 kg of CO_2 during that period which is twice the amount of maximum injection proposed in the project. The gas injection pressure and the rates are selected to achieve the

Table 5
Simulation conditions of the scenarios presented in Table 4.

Initial Conditions	Boundary Conditions
Gas concentration: 2.0 mol/m^3 Displacement: 0.0 m Horizonal stress: 0.26 MPa Vertical stress: 0.6 MPa	Gas injection boundary conditions applied at the borehole walls: • Fixed pressure (B1): 0.5 MPa (207.6 mol/m^3) • High injection rate (B2): 2 kg/h • Low injection rate (B3): 0.5 kg/h External edges/ side boundaries: • Gas concentration: 2.0 mol/m^3 • Mechanical deformation: Constant volume condition

Table 6
Model parameters used to simulate the simulation scenarios presented in Table 4.

Parameters	Values	References
Intrinsic permeability, m^2	8.16×10^{-16}	(Reeves and Taillefert, 2002)
Initial fracture porosity, n_{f0},-	0.006	(Staúczyk et al., 2012)
Coal density, ρ_s, kg/m^3	1470	(Staúczyk et al., 2012)
Residual saturation, Sr	0.003	(Staúczyk et al., 2012)
Matrix porosity, n_m,-	0.055	(Rodrigues and De Sousa, 2002)
Gas viscosity,μ_g, Pa·s	1.84×10^{-5}	(Haynes, 2014)
Diffusion coefficient in fractures, D, m^2/s	1.1×10^{-5}	(Haynes, 2014)
Fracture compressibility, C_f, MPa^{-1}	0.0082	(Li et al., 2013)
Henry's coefficient for CO_2, H_g, -	0.0347	(Sander, 2015)
Bulk elastic modulus, E, GPa	2.3	(Bukowska, 2005)
Matrix Young's modulus, E_m, GPa	11.5	(Hol and Spiers, 2012)
Modulus of solid, E_s, GPa	infinite	Given
Poisson's ratio, -	0.3	(Loschetter et al., 2012)
Langmuir pressure constant for CO_2, p_L, MPa	0.97	(Loschetter et al., 2012)
Langmuir volume constant for CO_2, C_L, mol/kg	1.69	(Loschetter et al., 2012)
Sorption time, τ, day	1.0	Given

target injection, as well as taking into account the equipment and facilities available at the EMB.

A summary of the simulation scenarios incorporating the trial design concepts and the injection conditions is presented in Table 4.

4.4. Domain discretisation (finite element meshing)

The simulation domain for Design 1, Packer-and-Port concept, is presented in Fig. 7a. The 10 m by 2 m by 2 m domain includes a 5 m long horizontal injection well with a diameter of 0.026 m. In this concept, the injection ports are operated individually and successively. Herein, gas injection is initiated from a point source, i.e., Port 1 (Fig. 6a), which is located at the bottom of the injection well (Fig. 7a). The simulation scenarios, D1B2 and D1B3, are designed to investigate the propagation of gas in the domain from the first injection port and to assess the distance (d_p) to the next port, *e.g.*, Port 2. The model domain is discretised using 3D tetrahedra mesh elements (Fig. 7b).

The model domains for Design 2 – 4 are presented Table 4, and the construction of the simulation domains is detailed in Fig. 8. The total length (L_T) varies depending on the length of the injection well, particularly, on the coal-CO_2 contact or (L_i) (Fig. 8a and 8b). The model domains are large and therefore computationally expensive to simulate using finite element method. However, owing to the symmetry, just a quarter of the domain is required to be solved (Fig. 8b). Each simulation domain includes a 10 m cased well and a 25 m intact coal seam together with L_i along the length of the seam (y-direction) (Fig. 8a and 8b). The width of the simulation domains is 17.5 m along x-axis and the thickness/depth is 1.0 m along z-axis. The diameter of the injection well is 0.02 m. The simulation domains are discretised using tetrahedra mesh elements (Fig. 8c). The selected points P1 to P4 along z-axis, and S1 to S4 along x-axis, are the locations of the simulation results observation points. Since no major faults or geological fissures exists in the study area, the coal seam at the simulation domains can be treated as a classic dual-porosity system, *i.e.*, fracture networks and matrix blocks.

4.5. Simulation conditions and model parameters

The initial and boundary conditions of the simulations are presented in Table 5 and the model parameters in Table 6. The geological background of the site is described in Section 2. The model conditions represent the 'seam-310' at 30 m depth, for example, horizontal and vertical stresses, moisture content etc. The overburden strata and the surrounding host rock formation is highly impermeable to fluid flow. Since no methane is detected in the site, it has been ignored in the simulations. Data related to the general characteristics of the coal at the EMB site are available through the past projects, e.g., RECOPOL (Reeves and Taillefert, 2002), HUGE (Staúczyk et al., 2012), and, where necessary, additional parameter values are obtained from literatures relevant to sub-bituminous coal.

5. Results

5.1. Simulation scenarios analysis

The simulation results are summarised for fracture gas pressure, adsorbed gas concentration at the matrix, and fracture permeability behaviour. The simulations runtime was 180 days. Please note that the permeability loss results presented in this paper combines the mean effective stress and CO_2 adsorption-induced coal swelling (for low pressure gas injection, the effective stress is smaller).

5.1.1. Scenarios: D1B2, D1B3

Evolution of CO_2 pressure in the study domain during D1B3 simulation (Packer-and-Port design concept) is presented in Fig. 9. It shows that the gas spreads nearly uniformly to the entire domain (from the source) and, therefore, possibly invalidates the concept of zonal

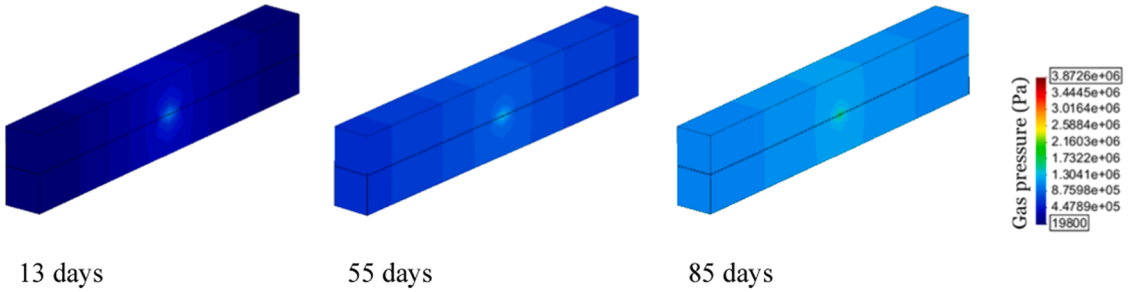

Fig. 9. Gas pressure evolution in the Design 1 study domain during the D1B3 simulation scenario. Point source injection from Port 1 of the Packer-and-Port design concept (Fig. 6a).

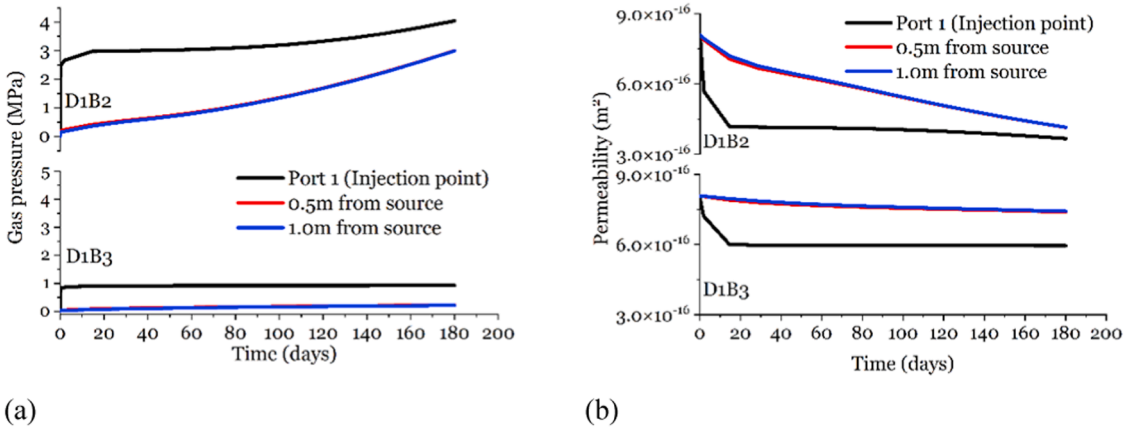

Fig. 10. (a) Gas pressure and (b) permeability evolution at the point of injection as well as at 0.5 m and 1.0 m from the source for D1B2 and D1B3 simulation scenarios.

isolation for incremental coal-CO_2 contact. To design the injection system, it is important to estimate the location of the next port (and packer), d_p, from the first injection point or Port 1 (Fig. 6a). Therefore, the gas pressure evolution at 0.5 m and 1.0 m from the injection point is monitored and compared with the source evolution (Fig. 10a) with the intent that d_p can be equated to either 0.5 m or 1.0 m. The results show that the gas pressure developments at these locations are almost identical in both simulations scenarios (D1B2 and D1B3). The simulated maximum gas pressure at these locations is 2.9 MPa during D1B2 scenario, whilst at the injection point it is 4.05 MPa. In D1B3 simulation, these values are 0.22 MPa and 0.92 MPa, respectively. In addition, no lag in the gas pressure developments between the successive locations is noticeable. Therefore, the distance between the packers or the ports cannot be calculated in a meaningful way. The permeability evolution results in Fig. 10b shows a 54.6% swelling-induced loss of permeability at the injection point in D1B2 scenario. Moreover, the permeability at 0.5 m away from the source is also reduced by 48.76% due to the source injection, *i.e.*, Port 1. For D1B3 simulation, these reductions are 26% and 8.16%, respectively. This means that the gas injectivity of the successive ports will be affected by the injection from the first port (both by the adsorbed CO_2 and the loss of permeability), and a sustained injection rate for individual ports will be challenging to establish. Therefore, the application feasibility of the Packer-and-Port concept in this context is questionable and will be analysed further in Section 6.

5.1.2. Scenarios: D2B1, D2B2, D2B3

The results of Design 2 simulation scenarios are presented in Fig. 11, and Figs. A1, A2 of Supporting Information. The results show that the CO_2 pressure increases rapidly at the locations closer to the injection well (P1) when fixed pressure boundary is applied [D2B1]. Away from the injection well, *e.g.*, at P3, P4, and S1-4, the pressure increase is slower. The maximum concentration of adsorbed gas at the observation points in the coal matrix for the D2B1 scenario is 845 mol/m^3. The corresponding permeability loss is 17.7%, from 8.16 $\times$ 10^{-16} m^2 to 6.75 $\times$ 10^{-16} m^2. In comparison, the values are lower for both injection rate boundary scenarios. The maximum gas pressures and adsorbed gas concentrations at the observation points in D2B2 and D2B3 simulations are respectively 0.275 MPa and 0.116 MPa, and 535 mol/m^3 and 256 mol/m^3. The corresponding permeability losses are 11.1% and 5.1%. Fig. A2 results show that the gas reaches to the S4 observation point, which is 10 m away from the source, after 100 days in D2B1 scenario. Meanwhile in D2B2 scenario the spread is up to S3, which is 5 m away from the source. The lowest spread is observed in D2B3 scenario.

5.1.3. Scenarios: D3B1, D3B2, D3B3

The results of Design 3 scenarios are presented in Fig. 12, and Figs. A3, A4 of Supporting Information. The fixed pressure boundary simulation results of D3B1 are same as that of the D2B1. The coal-CO_2 contact area (L_i) in this set of simulations is double than the previous scenarios. Therefore, for the same gas injection rates (B2 and B3), the mass flux per square meter area per unit time is lower than the Design 2 simulations. The maximum gas pressure and adsorbed gas concentration, at the observation points, calculated in D3B2 and D3B3 simulations are 0.165 MPa and 0.07 MPa, and 365 mol/m^3 and 170 mol/m^3, respectively. The corresponding fracture permeability values are 7.55 $\times$ 10^{-16} m^2 and 7.9 $\times$ 10^{-16} m^2. In comparison to the D2B2 results, the D3B2 results are 40% lower in CO_2 pressure, and 31.78% lower in adsorbed gas concentration. While 11.1% loss of permeability is calculated in the D2B2 scenario, in D3B2, the permeability loss is 7.5% (of the initial *in-situ* permeability). Similar comparison between D2B3 and D3B3 results shows 39.6% lower pressure and 33.6% lower adsorbed gas concentration. The loss of permeability in D3B3 simulation is 3.18% from the initial in-situ permeability (8.16 $\times$$10^{-16}$ m^2). Fig. A4 results show that it takes 90 days for CO_2 to spread to S3 observation point, located 5 m away from the source, during the D3B2 simulation. The propagation in the D3B3 simulation is observed at 2.0 m from the source (S2) but not at point S3.

5.1.4. Scenarios: D4B1, D4B2, D4B3

The results of Design 4 simulation scenarios are presented in Fig. 13 and Figs. A5, A6 of Supporting Information. The fixed pressure boundary simulation results of D4B1 are same as that of the D2B1 and D3B1. The coal-CO_2 contact area (L_i) in this set of simulations is four times larger than the D2-scenarios or twice than the D3-scenarios. The maximum gas pressure and adsorbed gas concentration calculated in D4B2 and D4B3 simulations are 0.11 MPa and 0.058 MPa, and 250 mol/m^3 and 116 mol/m^3, respectively. The corresponding fracture permeability values are 7.75 $\times$ 10^{-16} m^2 and 8.02 $\times$ 10^{-16} m^2. In comparison to the D2B2 results, the D4B2 results are 60% lower in CO_2 pressure, and 53.27% lower in adsorbed gas concentration. While 11.1% loss of permeability was estimated in the D2B2 scenario, in this case, the permeability loss is 5.02% (of the in-situ permeability) which is approximately 6% less than the D2B2 scenario and 2.4% less than the D3B2 scenario. Similar comparison between D2B3 and D4B3 results shows 50% lower pressure, and 54.68% lower adsorbed gas concentration. The loss of permeability in the D4B3 simulation is only 1.72% from the in-situ permeability (8.16 $\times$ 10^{-16} m^2). The mass flux of CO_2 in this set of simulations is the lowest which results in the smallest propagation of CO_2 into the domain. Fig. A6 results show that the spread is largely limited within 2 m distance from the source. Only a slight increase in gas pressure is observed at the S3 location (5 m from the source) in the D4B2 scenario near the end of the simulation period.

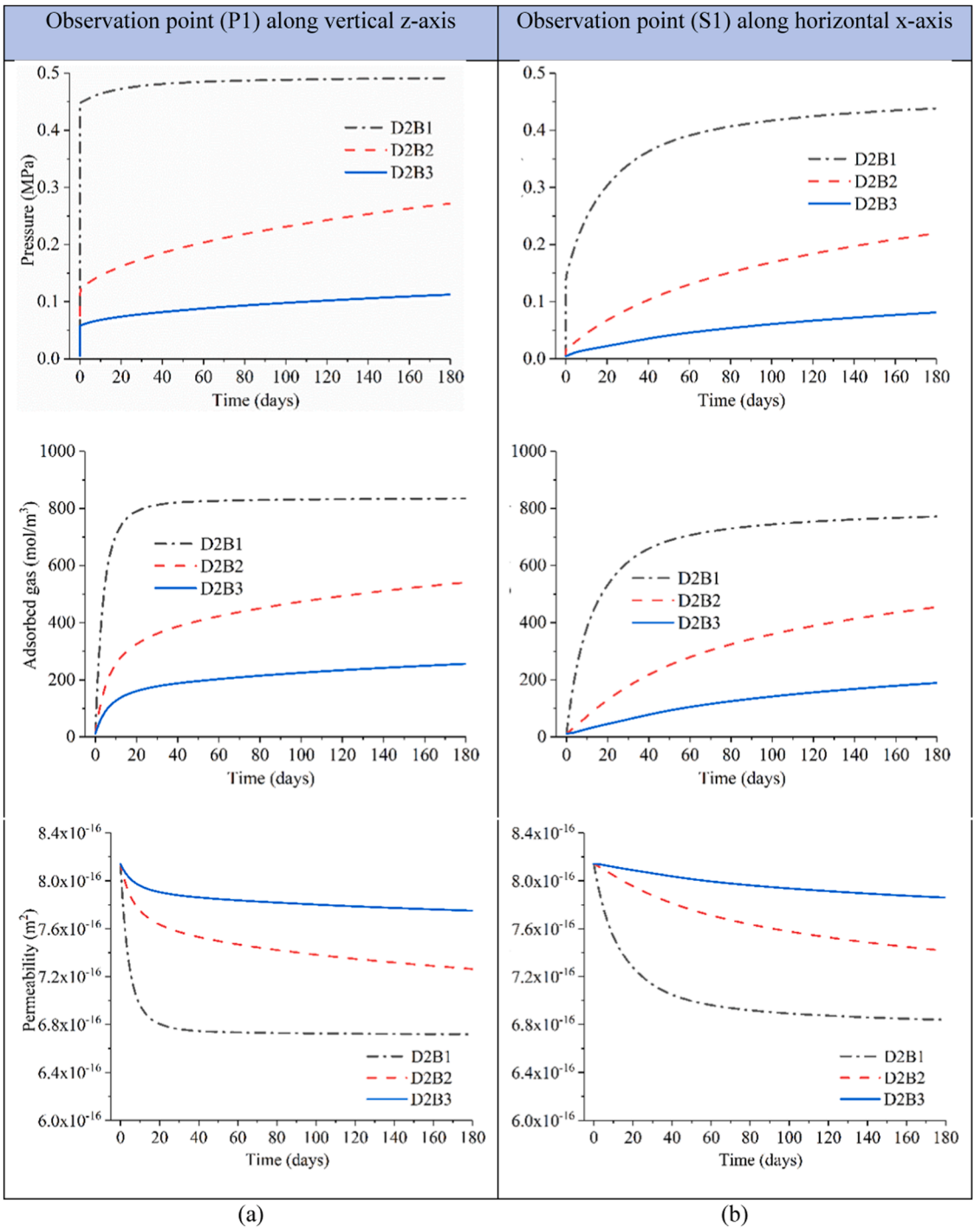

Fig. 11. Evolution of gas pressure, adsorbed gas concentration, and permeability at (a) P1 and (b) S1 observation points for Design 2 concept. Please note that the results of points P2-P4 and S2-S4 are presented in Fig. A1 and A2 of Supporting Information.

5.2. Influence of coal-CO_2 contact area

A summary of the key findings of variable coal-CO_2 contact area is presented in Fig. 14. It shows that the highest permeability loss is 17.7% when CO_2 is injected at 5 bar fixed pressure. The high injection rate B2 (2.0 kg/h) yields 11.1% loss of permeability, for the 25 m coal-CO_2 contact, which reduces further with the increasing contact lengths. For the low B3 injection rate the permeability loss is marginal (only 1.72%).

The maximum concentration of adsorbed CO_2 in the coal matrix is calculated to be 845 mol/m^3 or 1428 mol/kg for the fixed 5 bar gas injection condition. At the B2 injection rate, the observed maximum concentration is 535 mol/m^3 for the 25 m coal-CO_2 contact length. For the same injection rate, when the contact length is doubled and quadrupled the maximum adsorbed concentration is reduced to 365 and 250 mol/m^3, respectively. Therefore, by doubling the coal-CO_2 contact length, the adsorbed concentration is reduced by 31.7%, whereas a fourfold increase in the contact length reduces the concentration by 53.27%. This is because CO_2 mass flux per square meter of injection well is smaller for longer coal-CO_2 contact and larger for shorter coal-CO_2 contact, given that the rate of injection is same. Meanwhile, at the B3 injection rate that is 1/4th of the rate of B2, the 25 m, 50 m, and 100 m coal-CO_2 contact results into 256, 170, and 116 mol/m^3 maximum

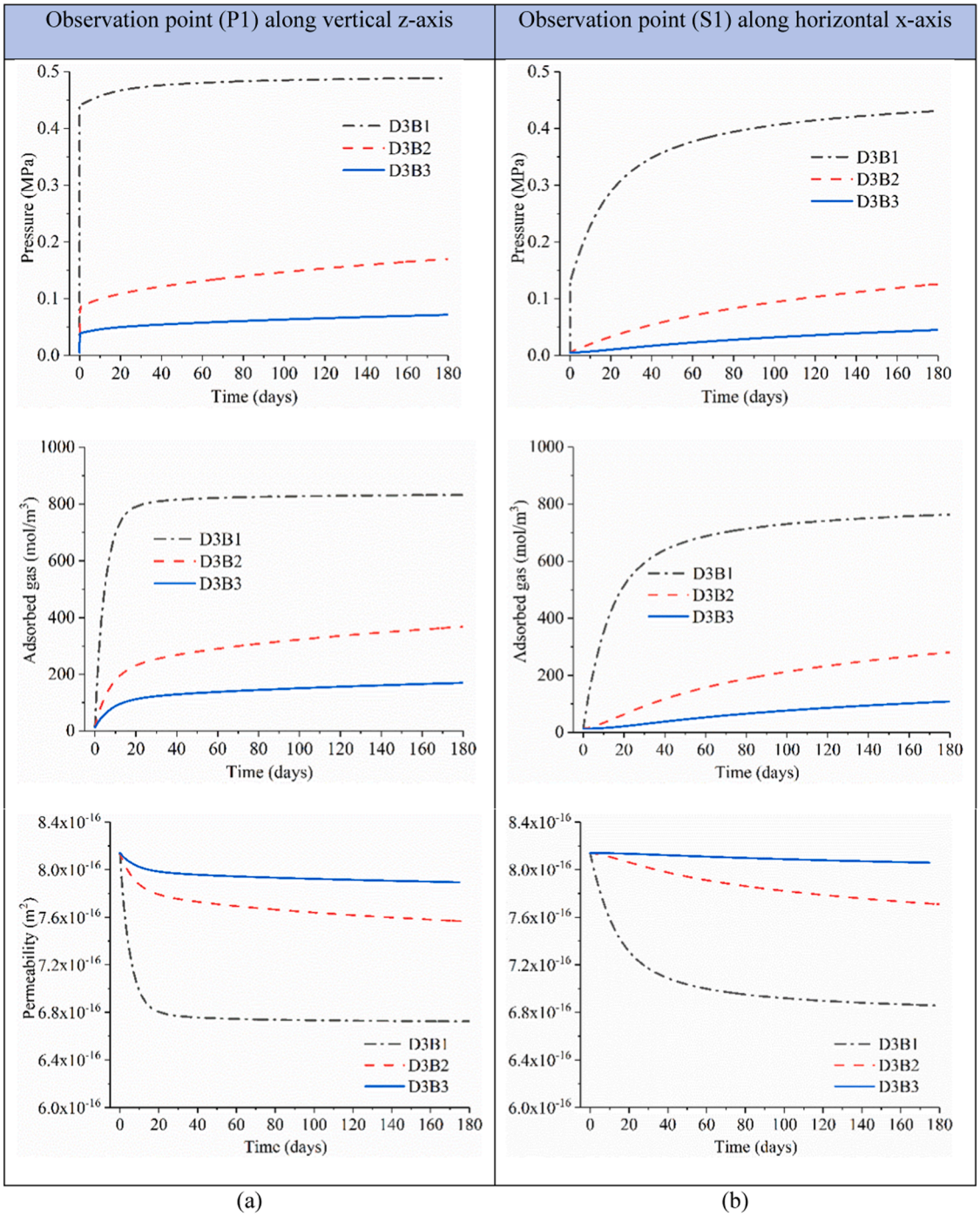

Fig. 12. Evolution of gas pressure, adsorbed gas concentration, and permeability at (a) P1 and (b) S1 observation points for Design 3 concept. Please note that the results of points P2-P4 and S2-S4 are presented in Fig. A3 and A4 of Supporting Information.

adsorbed CO_2 concentrations. These correspond to a reduction of adsorbed concentration by 52.1%, 53.4%, 53.6%, respectively. Therefore, a fourfold reduction in gas injection rate for a particular coal-CO_2 contact length results into roughly 53% reduction in adsorbed gas concentration. However, such a specific relationship between coal-CO_2 contact and permeability loss could not be established.

5.3. Spread of CO_2 in the model domain

An important aspect of geological CO_2 sequestration is to assess the propagation of the injected gas in the surrounding geology. The results of Design 1, Packer-and-Port concept, showed that the injected gas from point-source injection ports spread uniformly in the entire domain without any zonal isolation. Herein, the CO_2 spread in Design 2, 3, and 4 simulation scenarios are analysed in detail. As the simulation progresses, CO_2 propagates from the injection well to the model domain, adsorbs in the coal matrix, and drives the swelling-induced loss of permeability. Evolutions of gas pressure, adsorbed gas concentration, and permeability along the horizontal x-axis direction are detailed in Fig. 11(b), 12(b), 13(b) and Figs. A2, A4, A6 of Supporting Information. The end-of-simulation permeability contours are summarised in Fig. A7 of Supporting Information, and the corresponding gas pressure profiles are in Fig. 15. Under the fixed pressure boundary, for all alternative design concepts, the spread of gas is 12 m from the injection well, which is also

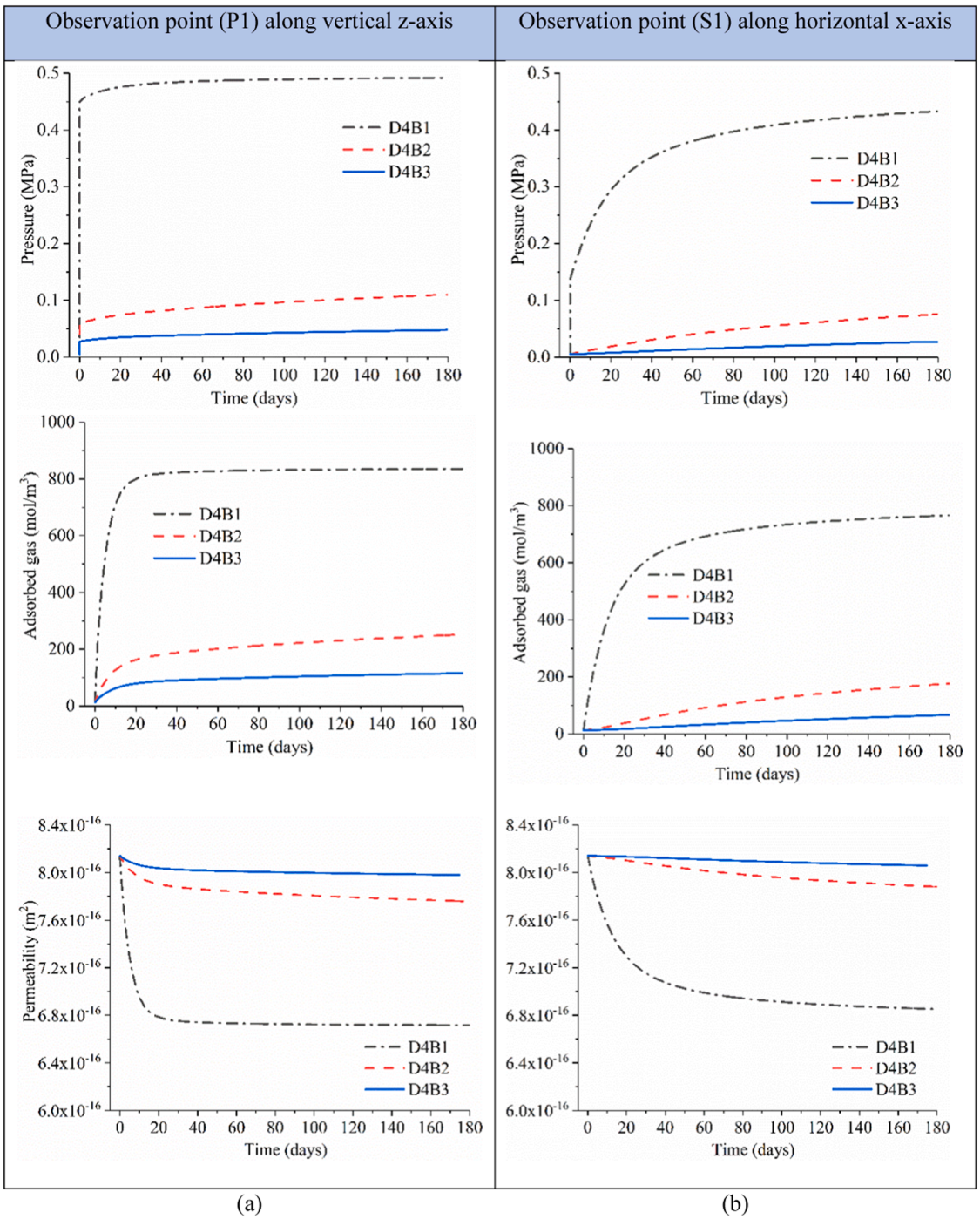

Fig. 13. Evolution of gas pressure, adsorbed gas concentration, and permeability at (a) P1 and (b) S1 observation points for Design 4 concept. Please note that the results of points P2-P4 and S2-S4 are presented in Fig. A5 and A6 of Supporting Information.

the maximum spread observed in the simulations. However, under the constant injection rates, B2 and B3, the gas propagation reduces with the coal-CO_2 contact length. The maximum spread during the B2 condition, is 7.2 m, 5.4 m, and 3.7 m for 25 m, 50 m, and 100 m coal-CO_2 contact lengths, respectively. The corresponding spreads in B3 conditions are 4.0 m, 3.3 m, and 2.3 m. Together with the analysis presented in the previous section, this suggests that the targeted amount (between 1 to 10 tonnes) of CO_2 can be injected in the seam steadily, without significant concerns of propagation in the domain.

The spread of CO_2 along the thickness of the seam (z-axis) is also calculated. The P4 observation point (z = 1.0 m) is located at the edge of the coal seam, *i.e.*, at the interface of the host rock. The maximum pressure calculated at P4 is 0.45 MPa during the B1 pressure boundary simulations (Fig.A1). In the B2 and B3 injection rate simulations, the highest simulated pressure at P4 is 0.24 MPa (D2B2) (Fig.A1) and the lowest pressure is 0.032 MPa (D4B3) (Fig.A5). Therefore, the coal-CO_2 contact length and the injection conditions could be regulated for upward movement of gas from the injection well. It is important to mention that the host rock or the overburden strata at the EMB (which consists of both carbonaceous and non-carbonaceous silt layers) is highly impermeable and provide sufficient insulation to upward gas flow (Staúczyk et al., 2012).

The extent of gas spread along the y-axis or along the length of the seam for Design 2 simulation scenarios are presented in Fig. 16. The

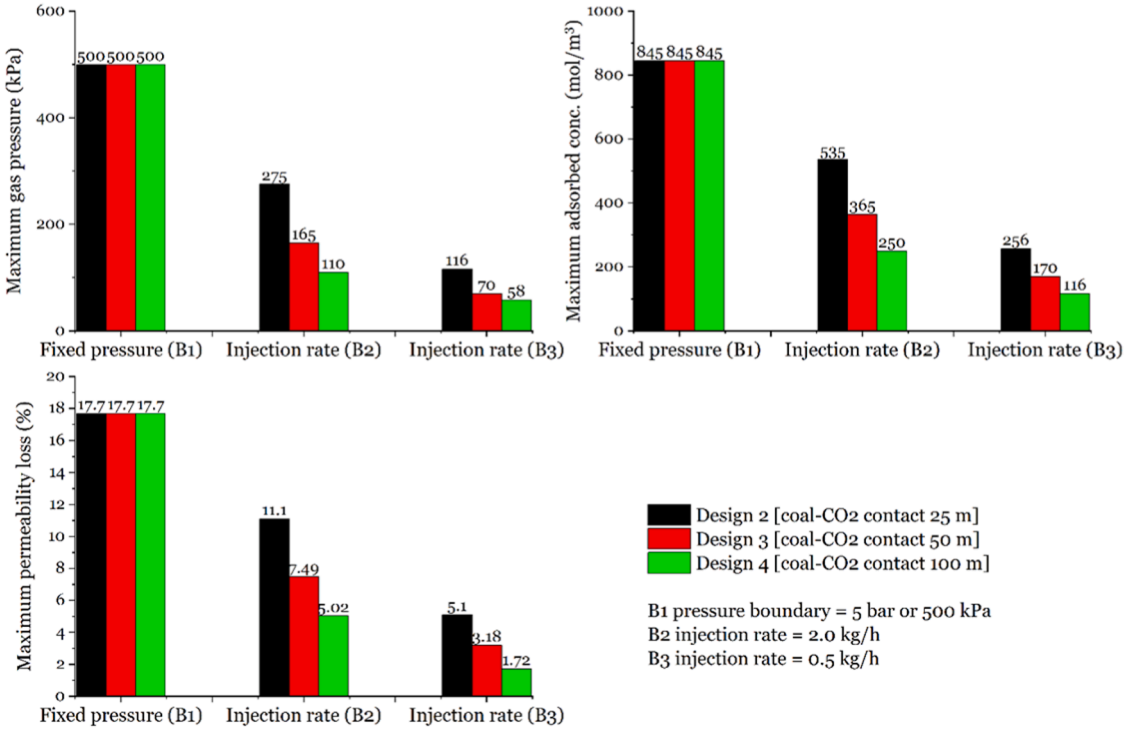

Fig. 14. Summary of the maximum gas pressure, adsorbed CO_2 concentration, and permeability loss calculated at the observation points from the Design 2, 3, and 4 simulation scenarios.

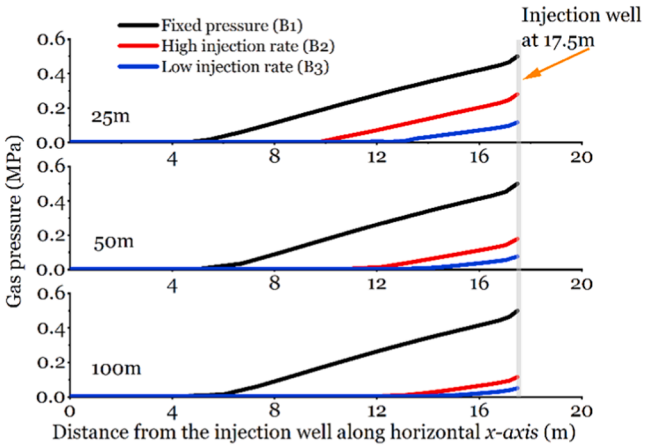

Fig. 15. Gas pressure profiles along the horizontal x-axis at the end of the 6-month simulation period. Fixed pressure B1 = 5 bar, Injection rate B2 = 2.0 kg/h, and Injection rate B3 = 0.5 kg/h. Location of the injeciton well is at x = 17.5 m.

evolution of gas concentration profiles show that spread is limited to the first 45 m (from the top) of the injection well (including the casing), leaving at least 15 m of the intact seam in this study domain (total length, L_T of Design 2 simulation domain is 60 m). This suggest that staged drilling of the injection well for incremental control of the coal-CO_2 contact area, presented in the Fig. 6b, can be achieved in the test site following the alternative design concept. For a given $L_T = 100$ m, in the first stage of the operation, if 25 m coal-CO_2 contact area is utilised for gas injection then, from the remaining length, at least another 40 or 50 m can be utilised in the successive operational stages. The operation can be continued for the entire length of a seam that is available/accessible for drilling.

5.4. Parameter sensitivity study

Sensitivity of the model parameters are also tested within the scope of this study. The model domain of Design 2, which includes a 25 m long coal-CO_2 contact length, is chosen as the simulation domain. The parameter sensitivity is analysed for the B2 gas injection boundary, *i.e.*, the D2B2 simulation scenario. The simulation conditions are presented in Table 5. The parameter values presented in Table 6 are considered as the base/reference values and the parameters, whose sensitivity are analysed, are listed in Table A3 of the Appendix. The focus here is on the structural and mechanical properties of the coal and the adsorption characteristics. The simulations duration was 6-months.

The summary of the parametric sensitivity simulations results is presented in Table S1 of the Supporting Information. The maximum gas pressure, adsorbed gas concentration, permeability loss, and gas spread observed in the simulations are compiled herein, to assess the sensitivity of the parameters of interest. The parameters are sorted according to their sensitivity in a Tornado diagram where the most sensitive parameters are placed at the top and the least sensitive parameters are at the bottom. From Table S1 and Fig. 17, it is evident that the most sensitive information for the model is the in-situ permeability, followed by the Langmuir pressure and volume constants. The least sensitive parameters are fracture porosity and diffusion time.

Since, permeability is the most sensitive parameter, its influence on gas pressure, adsorbed gas concentration, and permeability evolutions are analysed and in Fig. A8 of the Supporting Information. The results show that an order of magnitude increase in permeability, *i.e.*, $\kappa(10^{-16})$ to $\kappa(10^{-15})$, reduces the fracture gas pressure development by 56%, from 0.25 MPa to 0.11 MPa at P1 observation point (Fig. A8). Similar reduction is observed in the other obeservation points. The corresponding reductions in adsorbed gas concentration and permeability loss are 50.4% (from 535 to 265 mol/m^3) and 6.3% (from 11.1 % to 4.8% of the assinged in-situ permeability), respectively.

The profiles of adsorbed gas concentration and permeability with simulation time, along the horizontal x-axis direction, are presented in Fig. 18. The results indicate that an order of magnitude increase in

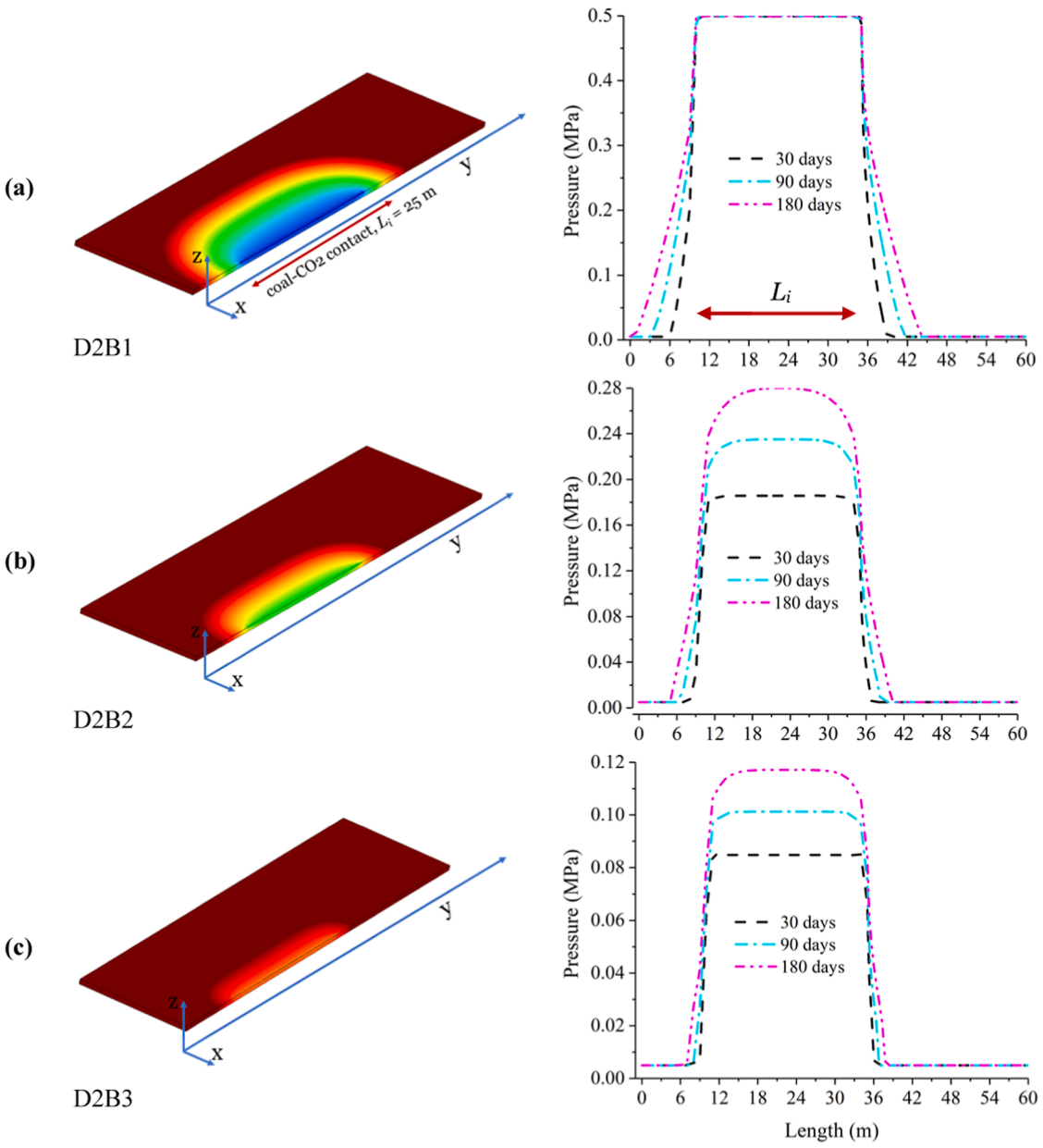

Fig. 16. Evolution of gas pressures along y-axis (or along the length of the seam) for Design D2 scenarios. Coal-CO_2 contact length 25 m. (a) Fixed pressure B1 = 5 bar, (b) Injection rate B2 = 2.0 kg/h, and (c) B3 = 0.5 kg/h.

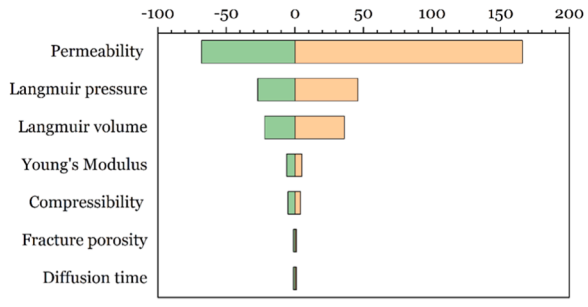

Fig. 17. Tornado diagram for analysing parametric sensitivity where the parameters are placed in descending sensitivity order. The most sensentive paramater is at the top while the least sensitive parameter at the bottom.

permeability increases the total CO_2 spread by 51%, from 7.2 m to 14.7 m. For two order of magnitude increase in permeability, *i.e.*, $\mathcal{O}(10^{-16})$ to $\mathcal{O}(10^{-14})$, however, the CO_2 spread exceeds the domain boundary. The analysis of the results suggest that at higher permeabilities gas pressure, adsorbed gas concentration, and permeability losses are reduced, but the propagation of the gas in the domain increases substantially. This highlights the importance of accurate site and seam-specific data, which will be available at a later stage of the project from field and laboratory studies, and will be included in the in-situ gas-injection operation and post gas-injection simulations.

6. Discussion

The results of Packer-and-Port design scenarios (Design 1) revealed that gas spreads to the entire test area from the first injection port and possibly undermines the concept of zonal isolation for incremental control of the coal-CO_2 contact area. Since the packers and the ports

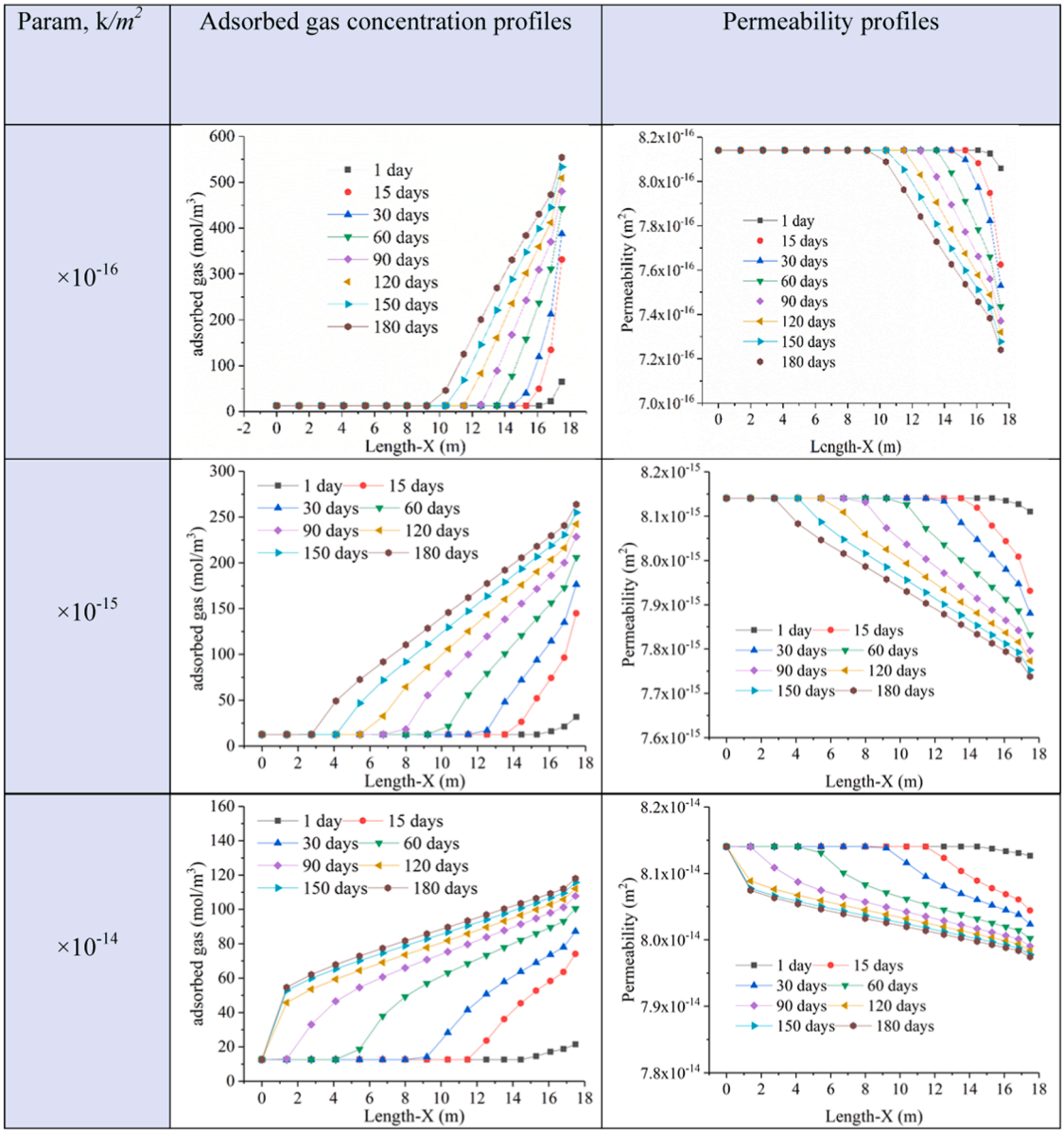

Fig. 18. Evolutions of adsorbed gas concentration and permeability profiles along the horizontal x-axis during the sensitivity simulations for the in-situ permeability. Parameter values Table 7 Case#1-3. The location of the injection well is at x = 17.5 m.

need to be controlled individually for effectively targeting specific areas of the seam, their individual distances should be known to design and construct the injection well (prior to the in-situ injection). However, the distances could not be calculated in a rational way. The simulation results highlighted that the CO_2 injected from a particular port altered the adsorbed gas concentration and permeability of the seam at the vicinity of the successive injection ports. That means only the first injection port encounters an intact or virgin seam whereas the successive ports will inject into an already CO_2-treated coal seam. Since coal permeability at the successive ports alters from the initial in-situ permeability and it also varies from port to port due to variable swelling-induced loss of permeability, sustained and appropriate gas injection rates for each port could not be established. As a result, the ports may remain underutilised or ineffective. If all injection ports are operated simultaneously, the concept becomes analogous to the alternative concepts tested in Design 2 to 4, which questions the use of expensive packer and ports in the injection system. Therefore, from a holistic perspective, the use of Packer-and-Port concept for regulating coal swelling, permeability, and gas injectivity associated with CCS in coal is not deemed feasible.

The alternative design scenarios, Design 2 to 4, demonstrated that the targeted amount (between 1 and 10 tonnes) of CO_2 could be either injected or exceeded into the seam without suffering from swelling-induced permeability loss and injectivity loss. The estimated maximum permeability loss in Packer-and-Port design is 54.6%, whereas in the alternative designs the maximum loss is 17.7%. This highlights the advantage of using the alternative stagged-drilling concept over the Packer-and-Port concept. Three different lengths of coal-CO_2 contact, *e.g.*, 25 m, 50 m, and 100 m, were investigated for three different injection conditions, and all scenarios revealed convincing results. The concept is also more flexible from design and operation perspective. Moreover, the alternative injection wells are based on conventional borehole drilling techniques rather than a complex and expensive Packer-and-Port system, and it can be implemented in the test site more conveniently.

The opportunity to expand the coal-CO_2 contact area along the length of the seam is the most beneficial aspect of using horizontal wells. Three design concepts are assessed for allowing increasing coal-CO_2 contact to provide useful insight to the swelling-induced loss of

permeability and gas injectivity. The model predicted highest permeability loss is 17.7%, at 5 bar fixed pressure CO_2 injection, which is significantly lower than the 93.7% permeability loss observed for the anthracite coal in Fig. 3. In all cases of staged drilling simulation scenarios, the amount of proposed CO_2 injection is either achieved or exceeded which suggest that by adjusting the coal-CO_2 contact area and the injectivity, permeability of the seam could be regulated to a desired levels and sustained gas injection rates could be achieved.

An important aspect of geological CO_2 sequestration is to assess its spread in the surrounding geology. Simulation results suggest that the targeted amount (between 1 to 10 tonnes) of CO_2 can be injected in the seam steadily, without significant risk of gas propagation. Analyses of the results along x, y, and z axis directions indicate adequate usage of coal reserves adopting the proposed injection well configuration, which is often challenging and impractical under vertical injection well concept.

7. Conclusion

This paper presents a pre-operational numerical simulation study for assisting design and operation of an in-situ CO_2 injection test facility in a shallow-depth coal seam. The seam is located 30 m below the surface at the Experimental Mine Barbara (EMB) in Mikołów, Poland. The coal is sub-bituminous, and the seam is already de-methanised. The in-situ test is intended to address and overcome swelling-induced permeability loss and injectivity issues, experienced in the past pilot projects on coal seam carbon storage. Utility of horizontal injection wells that utilises the natural orientation of coal cleat system and allow enlarged coal-CO_2 contact area is investigated. Pilot CO_2 injection tests in shallow-depth coal seams, using horizontal injection wells, are rarely attempted. Therefore, the current study provides useful insights on sub-critical CO_2 injection strategy and storage behaviour of such coal deposits. In the model, coal cleat networks and matrices are conceptualised as a dual-porosity system. Theoretical background of the model including CO_2 transport, coal-CO_2 interactions, and associated geomechanical processes are detailed in this paper. The model was tested against a CO_2 adsorption-induced coal swelling and permeability loss experiment. Simulated results agreed well with the experimental results demonstrating its reliability on predicting gas transport behaviour in coal as well as coal-CO_2 interactions. Several site-specific simulation scenarios were developed to evaluate various injection well configurations and operation conditions. The aim was to achieve injection of target CO_2 amount in the test seam effectively and efficiently. Two injection-well concepts, e.g., Packer-and-Port and stagged drilling were investigated for several gas injection conditions. To construct the model, full length of the injection well including the portion that is in direct contact with coal, and the cased portion near the mine gallery to stop gas leakage to the gallery are considered in a 3D model domain. Also, existing mine works and infrastructures were taken into account for a realistic representation of the test site. Simulation results were analysed and discussed in detail for gas pressure, adsorbed gas concentration, seam permeability evolutions as well as extent of gas propagation in the model domain. The following design recommendations and conclusions are drawn from the study:

- Staged drilling concepts, based on conventional horizontal borehole techniques, are more practical and certainly feasible than a Packer-and-Port injection concept for increasing coal-CO_2 contact interface and coal seam CO_2 storage. Injection wells of either 25, 50, or 100 m length could be exploited to achieve the target CO_2 injection (between 1000 to 10,000 kg of CO_2).
- A constant injection rate of 2.0 kg/h or 0.5 kg/h would lead to total 8640 kg or 2160 kg of CO_2 injection, respectively, in a period of 6-months. However, a fixed pressure injection of 5 bar would require roughly 3 months to inject 10,000 kg of CO_2 in the test site.
- The predicted maximum swelling-induced seam permeability loss is between 17 and 18% for the fixed pressure injection. The values are significantly less for the constant injection rates considered in this study. This suggests that a steady and sustained CO_2 injection operation could be established for the shallow in-situ test site without concerns of major permeability loss, which was often experienced in past projects that targeted deeper coal seams.
- The maximum predicted CO_2 spread in the study area is 12 m from the centre of the injection well (for the 5-bar fixed pressure condition). For the constant injection rates, 0.5 to 2.0 kg/h, the simulated spreads are within 4.0 to 7.2 m. This suggests that the proposed width of test area is adequate for the proposed CO_2 injection. The information is also useful to guide installations (locations) of the vertical monitoring wells in the test facility.
- The magnitude of CO_2 propagation along the length of the seam supports the staged or incremental drilling of the horizontal injection well, since the proportion of the CO_2-treated seam that could be disturbed by successive drilling is significantly small ($<$10 m in this study) comparting to the total available length of the seam. Gas spread in the transverse direction of the injection well could be controlled by regulating the coal-CO_2 contact length and operating conditions. A shorter contact length and higher injection rate would accelerate CO_2 spread, whereas a longer contact length with lower injection rate would reduce the spread.
- Sensitivity study of the model parameters revealed that the most sensitive site information is the in-situ permeability of the seam which is followed by the coal-CO_2 adsorption characteristics information. The data should be collected with greatest care.

CRediT authorship contribution statement

Shakil A. Masum: Conceptualization, Methodology, Formal analysis, Investigation, Writing – original draft, Writing – review & editing, Supervision, Visualization, Project administration, Funding acquisition. **Min Chen:** Methodology, Software, Validation, Formal analysis, Investigation, Resources, Visualization. **Lee J. Hosking:** Conceptualization, Formal analysis, Writing – review & editing. **Kamil Stańczyk:** Resources. **Krzysztof Kapusta:** Resources. **Hywel R. Thomas:** Writing – review & editing, Supervision, Project administration, Funding acquisition.

Declaration of Competing Interest

The authors declare that they have no known competing financial interests or personal relationships that could have appeared to influence the work reported in this paper.

Acknowledgment

The research was conducted as part of the “Establishing a Research Observatory to Unlock European Coal Seams for Carbon Dioxide Storage (ROCCS)” project and co-financed by the program of the Minister of Science and Higher Education entitled "PMW" in the years 2020-2023; (agreement No. 5144/FBWiS/2020/2). The ROCCS project has received funding from the Research Fund for Coal and Steel under Grant Agreement No. 899336. The financial supports are gratefully acknowledged.

Supplementary materials

Supplementary material associated with this article can be found, in the online version, at doi:10.1016/j.ijggc.2022.103725.

Appendix

Table A1,A2 A3

Table A1
Summary of pilot and demonstration projects of CO_2 injection into coal seams.

Country	Start	Project name/Location	tonnes CO_2	Depth (m)	References
USA	1995	Allison Unit, San Juan Basin, New Mexico	251,000	950	(IEAGHG, 2013)
Canada	1998	Fenn Big Valley, Alberta	200	1,200	(Gunter et al., 2005)
China	2004	Qinshui Basin, Shanxi Province	192	470	(Connell et al., 2014)
Japan	2004	Yubari, Ishikari Coalfield, Hokkaido	884	900	(Fujioka et al., 2010)
Poland	2004	RECOPOL/ Upper Silesian Basin, Poland	760	1,100	(RECOPOL 2006)
Slovenia	2006	MOVECBM/ Velenje Mine	0.0057	-	(van Wageningen et al., 2009)
USA	2008	Pump Canyon, San Juan Basin, New Mexico	16,700	900	(IEAGHG, 2013)
USA	2008	Tanquary Farms, Illinois Basin, Illinois	90	274	(IEAGHG, 2013)
USA	2009	Burke County, North Dakota	80	370	(IEAGHG, 2013)
China	2010	Qinshui Basin II, Shanxi Province	234	923	(Connell et al., 2014)
USA	2010	Blue Creek, Black Warrior Basin, Alabama	252	300-550	(IEAGHG, 2013)
China	2011	APP ECBM/Ordos Basin, Shanxi Province	460	560*	(Connell et al., 2014)
China	2013	Qinshui Basin III, Shanxi Province	4,491	972	(Connell et al., 2014)
Spain	2013	CARBOLAB/ Montsacro Pit, Asturias, Spain	0.12	550	(Lafortune et al., 2014)
USA	2015	Buchanan County, Central Appalachian Basin, Virginia	14,000	275-670	(IEAGHG, 2013)

* CO_2 injected using horizontal wells with total in seam length of 2,305 m.

Table A2
A comparison between past pilot tests in European coal and the ROCCS proposal.

Project	Well length, m	Sealing depth, m	In-seam Length, m	Depth, m	CO_2 injected, kg	Injection duration*
MOVECBM (van Wageningen et al., 2009)	30	25	5	400	5.7	30 hours
CARBOLAB (Lafortune et al., 2014)	30	15	6	550	120	2 months
ROCCS	100	25	75	30	1000 – 10000	3-6 months

* Duration of the injection phase ignoring stages and down-time.

Table A3
The parameters and their values used in the sensitivity analysis.

Case No.	k(m^2)	n_{f0}	C_f(MPa^{-1})	E(GPa)	p_L(MPa)	C_L(mol/kg)	τ(day)
1	8.16e-16	0.006	0.0082	2.3	0.97	1.69	1.0
2	8.16e-15	0.006	0.0082	2.3	0.97	1.69	1.0
3	8.16e-14	0.006	0.0082	2.3	0.97	1.69	1.0
4	8.16e-16	0.012	0.0082	2.3	0.97	1.69	1.0
5	8.16e-16	0.018	0.0082	2.3	0.97	1.69	1.0
6	8.16e-16	0.006	0.004	2.3	0.97	1.69	1.0
7	8.16e-16	0.006	0.012	2.3	0.97	1.69	1.0
8	8.16e-16	0.006	0.0082	1.0	0.97	1.69	1.0
9	8.16e-16	0.006	0.0082	3.5	0.97	1.69	1.0
10	8.16e-16	0.006	0.0082	2.3	0.97	1.69	1.0
11	8.16e-16	0.006	0.0082	2.3	2.0	1.69	1.0
12	8.16e-16	0.006	0.0082	2.3	3.0	1.69	1.0
13	8.16e-16	0.012	0.0082	2.3	0.97	1.0	1.0
14	8.16e-16	0.018	0.0082	2.3	0.97	2.5	1.0
15	8.16e-16	0.006	0.0082	2.3	0.97	1.69	0.5
16	8.16e-16	0.006	0.0082	2.3	0.97	1.69	2.0

References

IEAGHG. Potential Implications on gas production from shales and coals for geological storage of CO_2. https://ieaghg.org/docs/General_Docs/Reports/2013-10.pdf.

IPCC, 2018. In: Masson-Delmotte, V, Zhai, S, Pörtner, H-O, Roberts, D, Skea, J, Shukla, PR, Pirani, A, Moufouma-Okia, W, Péan, C, Pidcock, R, Connors, S, Matthews, JBR, Chen, Y, Zhou, X, Gomis, MI, Lonnoy, E, Maycock, T, Tignor, M, Waterfield, T (Eds.), Global warming of 1.5°C. An IPCC Special Report on the impacts of global warming of 1.5°C above pre-industrial levels and related global greenhouse gas emission pathways, in the context of strengthening the global response to the threat of climate change, sustainable development, and efforts to eradicate poverty. In Press.[cited 2021 July 10] Available at https://www.ipcc.ch/sr15/.

Metz, B, Davidson, O, Coninck de, H, Loos, M, Meyer, L, 2005. IPCC Special Report on Carbon Dioxide Capture and Storage. Cambridge University Press, New York, United States.

Vangkilde-Pedersen, T, Kirk, K, Smith, N, Maurand, N, Wojcicki, A, Neele, F, Hendriks, C, Nindre, Y-M L, Anthonsen, KL, 2009. Assessing European capacity for geological storage of carbon dioxide – the EU GeoCapacity project. Energy Procedia 1 (1), 2663–2670. https://doi.org/10.1016/j.egypro.2009.02.034.

Alves Dias, P, Kanellopoulos, K, Medarac, H, Kapetaki, Z, Miranda Barbosa, E, Shortall, R, Czako, V, Telsnig, T, Vazquez Hernandez, C, Lacal Arantegui, R, Nijs, W, Gonzalez Aparicio, I, Trombetti, M, Mandras, G, Peteves, E, Tzimas, E, 2018. EU coal regions: opportunities and challenges ahead. Publications Office of the European Union: Luxembourg. https://doi.org/10.2760/064809.

EU Geocapacity, 2008. EU Geocapacity - Assessing European Capacity for Geological Storage of Carbon Dioxide. Project no. SES-518318. Final report. https://ec.europa.eu/clima/sites/clima/files/docs/0028/geocapacity_en.pdf.

Sarhosis, V, Hosking, LJ, Thomas, HR, 2016. Carbon sequestration potential of the South Wales Coalfield. Environmental Geotechnics 5 (4), 234–246. https://doi.org/10.1680/jenge.16.00007.

RECOPOL, 2006. Reduction of CO_2 emission by means of CO_2 storage in coal seams in the Silesian Coal Basin of Poland (RECOPOL) project. Report Number 2006/10 Final Report. https://ieaghg.org/docs/General_Docs/Reports/2006-10%20Final%20RECOPOL%20Report.pdf.

Fujioka, M, Yamaguchi, S, Nako, M, 2010. CO_2-ECBM field tests in the Ishikari Coal Basin of Japan. Int. J. Coal Geol. 82 (3-4), 287–298. https://doi.org/10.1016/j.coal.2010.01.004.

Harpalani, S, Chen, G, 1997. Influence of gas production induced volumetric strain on permeability of coal. Geotech. Geol. Eng. 15, 303–325.

White, CM, Smith, DH, Jones, KL, Goodman, AL, Jikich, SA, LaCount, RB, DuBose, SB, Ozdemir, E, Morsi, BI, Schroeder, KT, 2005. Sequestration of carbon dioxide in coal with enhanced coalbed methane recovery a review. Energy Fuels 19 (3), 659–724. https://doi.org/10.1021/ef040047w.

Busch, A, Gensterblum, Y, 2011. CBM and CO_2-ECBM related sorption processes in coal: a review. Int. J. Coal. Geol. 87 (2), 49–71. https://doi.org/10.1016/j.coal.2011.04.011.

Cai, Y, Pan, Z, Liu, D, Zheng, G, Tang, S, Connell, LD, Yao, Y, Zhou, Y, 2014. Effects of pressure and temperature on gas diffusion and flow for primary and enhanced

coalbed methane recovery. Energy Exploration and Exploitation 32 (4), 601–619, 10.1260.2F0144-5987.32.4.601.
Pone, JDN, Halleck, PM, Mathews, JP, 2009. Sorption capacity and sorption kinetic measurements of CO_2 and CH_4 in confined and unconfined bituminous coal. Energy Fuels 23 (9), 4688–4695. https://doi.org/10.1021/ef9003158.
Perera, MSA, Ranjith, PG, Peter, M, 2011. Effects of saturation medium and pressure on strength parameters of Latrobe Valley brown coal: carbon dioxide, water and nitrogen saturations. Energy 36 (12), 6941–6947. https://doi.org/10.1016/j.energy.2011.09.026.
Perera, MSA, 2017. Influences of CO_2 injection into deep coal seams: a review. Energy Fuels 31, 10324–10334. https://doi.org/10.1021/acs.energyfuels.7b01740.
Walker, PL, Verma, S, Rivera-Utrilla, J, Khan, MR, 1988. A direct measurement of expansion in coals and macerais induced by carbon dioxide and methanol. Fuel 67 (5), 719–726. https://doi.org/10.1016/0016-2361(88)90305-5.
Ammosov, II, Eremin, IV, 1963. Fracturing in coal. IZDAT Publishers, Moscow.
Tremain, CM, Laubach, SE, Whitehead, NH, 1991. Coal fracture cleat patterns in Upper Cretaceous Fruitland Formation, San Juan Basin, Colorado and New Mexico: implications for exploration and development. Coalbed methane of Western North America. Rocky Mountain Association of Geologists, pp. 49–59. In: Schwochow S, Murray DK, Fahy MF (eds).
Laubach, SE, Marrett, R, Olson, J, Scott, AR, 1998. Characteristics and origins of coal cleat: a review. Int. J. Coal. Geol. 35, 175–207. https://doi.org/10.1016/S0166-5162(97)00012-8.
Su, X, Feng, Y, Chen, J, Pan, J, 2001. The characteristics and origins of cleat in coal from Western North China. Int. J. Coal. Geol. 47 (1), 51–62. https://doi.org/10.1016/S0166-5162(01)00026-X.
Gentzis, T, Bolen, D, 2008. The use of numerical simulation in predicting coalbed methane producibility from the Gates coals, Alberta inner Foothills, Canada: comparison with Mannville coal CBM production in the Alberta Syncline. Int. J. Coal. Geol. 74, 215–236. https://doi.org/10.1016/j.coal.2007.12.003.
Ren, J, Ren, J, Zhang, L, Ren, S, Lin, J, Meng, S, Ren, G, Gentzis, T, 2014. Multi- branched horizontal wells for coalbed methane production: field performance and well structure analysis. Int. J. Coal. Geol. 131, 52–64. https://doi.org/10.1016/j.coal.2014.06.003.
Sheng, JJ, 2017. Optimization of huff-n-puff gas injection in shale oil reservoirs. Petroleum 3 (4), 431–437. https://doi.org/10.1016/j.petlm.2017.03.004.
Zhang, J, Feng, Q, Zhang, X, Hu, Q, Wen, S, Chen, D, Zhai, Y, Yan, X, 2020. Multi-fractured horizontal well for improved coalbed methane production in eastern Ordos basi, China: field observations and numerical simulations. Journal of Petroleum Science and Engineering 194, 107488. https://doi.org/10.1016/j.petrol.2020.107488.
Connell, L, Pan, Z, Camilleri, M, Shangzhi, M, Down, D, Carras, J, Wenzhong, Z, Xiaokang, F, Benguang, G, Briggs, C, Lupton, N, 2014. Description of a CO_2 enhanced coal bed methane field trial using a multi-lateral horizontal well. Int. J. Greenhouse Gas Control 26, 204–219. https://doi.org/10.1016/j.ijggc.2014.04.022.
Kapusta, K, Stanczyk, K, Wiatowski, M, Checko, J, 2013. Environmental aspects of a field-scale underground coal gasification trial in a shallow coal seam at the Experimental Mine Barbara in Poland. Fuel 113, 196–208. https://doi.org/10.1016/j.fuel.2013.05.015.
van Wageningen, WFC, Wentinck, HM, Otto, C, 2009. Report and modeling of the MOVECBM field tests in Poland and Slovenia. Energy Procedia 1 (1), 2071–2078. https://doi.org/10.1016/j.egypro.2009.01.270.
Lafortune, S, Adelise, F, Bentivegna, G, Didier, C, Farret, R, Gombert, P, Lagny, C, Pokryszka, Z, Toimil, NC, 2014. An experimental approach to adsorption of CO_2+CH_4 gas mixtures onto coal (European RFCS CARBOLAB research project). Energy Procedia 63, 5870–5878. https://doi.org/10.1016/j.egypro.2014.11.620.
Fabiańska, MJ, Smółka-Danielowska, D, 2012. Biomarker compounds in ash from coal combustion in domestic furnaces (Upper Silesia Coal Basin, Poland). Fuel 102, 333–344. https://doi.org/10.1016/j.fuel.2012.07.012.
Thomas, HR, He, Y, 1995. Analysis of coupled heat, moisture and air transfer in a deformable unsaturated soil. Géotechnique 45 (4), 677–689. https://doi.org/10.1680/geot.1995.45.4.677.
Thomas, HR, Seetharam, SC, Vardon, PJ, 2011. On the inclusion of some biological impacts and influences in coupled transport phenomena in unsaturated soil. Geotech. Geol. Eng. 29, 181–191. https://link.springer.com/article/10.1007%2Fs10706-010-9316-6.
Masum, SA, 2012. Modelling of reactive gas transport in unsaturated soil. A coupled thermo-hydro-chemical-mechanical approach. Cardiff University, UK. PhD Thesis. https://orca.cardiff.ac.uk/38159/.
Hosking, LJ, 2014. Reactive transport modelling of high pressure gas flow in coal. Cardiff University, UK. PhD Thesis. https://orca.cardiff.ac.uk/61446/.
Masum, SA, Thomas, HR, 2018. Modelling coupled microbial processes in the subsurface: model development, verification, evaluation and application. Adv. Water Resour. 116, 1–17. https://doi.org/10.1016/j.advwatres.2018.03.015.
Masum, SA, Thomas, HR, 2021. Effects of microbial spatial distribution on organic biodegradation and immobilization of trace metals in co-contaminated soils. Comput. Geotech. 133, 104063 https://doi.org/10.1016/j.compgeo.2021.104063.
Hosking, LJ, Chen, M, Thomas, HR, 2020. Numerical analysis of dual porosity coupled thermo-hydro-mechanical behaviour during CO_2 sequestration in coal. Int. J. Rock Mech. Min. Sci. 135, 104473 https://doi.org/10.1016/j.ijrmms.2020.104473.
Chen, M, Masum, S, Sadasivam, S, Thomas, H, 2022. Modelling anisotropic adsorption-induced coal swelling and stress-dependent anisotropic permeability. Int. J. Rock Mech. Min. Sci. 153, 105107 https://doi.org/10.1016/j.ijrmms.2022.105107.
Chen, M, 2019. Modelling of gas transport in coal - a hybrid coupled dual porosity and discrete fracture approach. Cardiff University. PhD Thesis. https://orca.cardiff.ac.uk/129350/.
Chen, M, Hosking, LJ, Sandford, RJ, Thomas, HR, 2019. Dual porosity modelling of the coupled mechanical response of coal to gas flow and adsorption. Int. J. Coal. Geol. 205, 115–125. https://doi.org/10.1016/j.coal.2019.01.009.
Chen, M, Hosking, LJ, Sandford, RJ, Thomas, HR, 2020a. A coupled compressible flow and geomechanics model for dynamic fracture aperture during carbon sequestration in coal. Int. J. Numer. Anal. Methods Geomech. 44 (13), 1727–1749. https://doi.org/10.1002/nag.3075.
Chen, M, Masum, SA, Thomas, HR, 2020b. Modelling non-isothermal transport behaviour of real gas in deformation coal matrix. Energy Fuels 25 (2), 1605–1619. https://pubs.acs.org/doi/full/10.1021/acs.energyfuels.0c03728.
Chen, M, Masum, SA, Thomas, HR, 2020c. Modelling adsorption and transport behaviour of gases in moist coal matrix. Energy Fuels. https://pubs.acs.org/doi/10.1021/acs.energyfuels.1c01334.
Peng, DY, Robinson, DB, 1976. A new two-constant equation of state. Ind. Eng. Chem. Fundam. 15 (1), 59–64. https://doi.org/10.1021/i160057a011.
Jaeger, JC, Cook, NG, Zimmerman, R, 2009. Fundamentals of rock mechanics. John Wiley & Sons.
Lewis, RW, Schrefler, BA, 1998. The finite element method in the static and dynamic deformation and consolidation of porous media. John Wiley & Sons.
Pao, WK, Lewis, RW, 2002. Three-dimensional finite element simulation of three-phase flow in a deforming fissured reservoir. Comput. Methods Appl. Mech. Eng. 191 (23-24), 2631–2659. https://doi.org/10.1016/S0045-7825(01)00420-0.
Lewis, RW, Pao, WK, 2002. Numerical simulation of three-phase flow in deforming fractured reservoirs. Oil and Gas Science and Technology 57 (5), 499–514. https://ogst.ifpenergiesnouvelles.fr/articles/ogst/pdf/2002/05/lewis_v57n5.pdf.
Chen, D, Pan, Z, Ye, Z, 2015. Dependence of gas shale fracture permeability on effective stress and reservoir pressure: model match and insights. Fuel 139, 383–392. https://doi.org/10.1016/j.fuel.2014.09.018.
Sampath, K, Perera, M, Ranjith, P, Matthai, S, 2019. CO_2 interaction induced mechanical characteristics alterations in coal: a review. Int. J. Coal. Geol. 204, 113–129. https://doi.org/10.1016/j.coal.2019.02.004.
Zagorscak, R, 2017. An investigation of coupled processes in coal in response to high pressure gas injection. Cardiff University, UK. PhD Thesis. https://orca.cardiff.ac.uk/100058/.
Chen, Z, Pan, Z, Liu, J, Connell, LD, Elsworth, D, 2011. Effect of the effective stress coefficient and sorption-induced strain on the evolution of coal permeability: experimental observations. Int. J. Greenhouse Gas Control 5 (5), 1284–1293. https://doi.org/10.1016/j.ijggc.2011.07.005.
Zheng, G, Pan, Z, Chen, Z, Tang, S, Connell, LD, Zhang, S, Wang, B, 2012. Laboratory study of gas permeability and cleat compressibility for CBM/ECBM in Chinese coals. Energy Exploration and Exploitation 30 (3), 451–476, 10.1260%2F0144-5987.30.3.451.
Peng, S, Fang, Z, Shen, J, Xu, J, Wang, G, 2017. Effects of gas sorption-induced swelling/shrinkage on the cleat compressibility of coal under different bedding directions. Sci. Rep. 7 (1), 1–10. https://www.nature.com/articles/s41598-017-14678-1.
Connell, LD, 2016. A new interpretation of the response of coal permeability to changes in pore pressure, stress and matrix shrinkage. Int. J. Coal. Geol. 162, 169–182. https://doi.org/10.1016/j.coal.2016.06.012.
Energy & Environmental Research Center, 2014. Completion Technologies. [cited 2021 July 2]; Available from: https://undeerc.org/bakken/completiontechnologies.aspx.
Reeves SR, Taillefert A, 2002. Reservoir modeling for the design of the RECOPOL CO_2 sequestration project, Poland. Topical Report, DOE Contract No. DE-FC26-00NT40924.
Staúczyk, K, Świądrowski, J, Kapusta, K, Howaniec, N, Cybulski, K, Rogut, J, Smoliński, A, Wiatowski, M, Kotyrba, A, Krause, E, Tokarz, A, Grabowski, J, Ludwik-Pardała, M, Bruining, J, Eftekhari, AA, Schuster, A, Solcova, O, Svoboda, K, Soukup, K, Landuyt, P, Garot, D, Śpiewak, T, Szarafiński, M, Niewiadomski, M, Budynek, P, Bednarczyk, AJ, Marek, A, Rzepa, S, Rogosz, B, Green, M, Palarski, J, Strozik, G, Falshtynky, V, Dychkowsky, R., 2012. Hydrogen-oriented undergound coal gasification for Europe (HUGE). Final Report. DGRI European Union, Luxembourg. https://doi.org/10.2777/9857.
Rodrigues, CF, De Sousa, ML, 2002. The measurement of coal porosity with different gases. Int. J. Coal. Geol. 48 (3-4), 245–251. https://doi.org/10.1016/S0166-5162(01)00061-1.
Haynes, WM, 2014. CRC handbook of chemistry and physics. CRC press.
Li, S, Tang, D, Pan, Z, Xu, H, Huang, W, 2013. Characterization of the stress sensitivity of pores for different rank coals by nuclear magnetic resonance. Fuel 111, 746–754. https://doi.org/10.1016/j.fuel.2013.05.003.
Sander, R, 2015. Compilation of Henry's law constants (version 4.0) for water as solvent. Atmos. Chem. Phys. 15 (8), 4399–4981. https://acp.copernicus.org/articles/15/4399/2015/acp-15-4399-2015.pdf.
Bukowska, M, 2005. Mechanical properties of carboniferous rocks in the Upper Silesian Coal Basin under uniaxial and triaxial compression tests. J. Min. Sci. 41 (2), 129–133. https://doi.org/10.1007/s10913-005-0073-5.
Hol, S, Spiers, CJ, 2012. Competition between adsorption-induced swelling and elastic compression of coal at CO_2 pressures up to 100 MPa. J. Mech. Phys. Solids 60 (11), 1862–1882. https://doi.org/10.1016/j.jmps.2012.06.012.
Loschetter, A, Smaï, F, Sy, S, Burnol, A, Leynet, A, Lafortune, S, Thoraval, A, 2012. Simulation of CO_2 storage in coal seams: coupling of TOUGH2 with the solver for mechanics CODE_ASTER®. In: The Proceedings of TOUGH Symposium, September 17-19, 2012. Lawrance Berkley National Laboratory.
Gunter, WD, Mavor, MJ, Robinson, JR, 2005. CO_2 storage and enhanced methane production: Field testing at Fenn-Big Valley, Alberta, Canada, with application. In: the proceedings of the 7th International Conference on Greenhouse Gas Control Technologies 5- September 2004. Vancouver, Canada.